Hydrodynamics of a high Alpine catchment characterized by four natural tracers

Anthony Michelon[1], Natalie Ceperley[2], Harsh Beria[3], Joshua Larsen[4,5], Torsten Vennemann[1], Bettina Schaefli[2]

[1]Institute of Earth Surface Dynamics (IDYST), Faculty of Geosciences and Environment (FGSE), University of Lausanne, Lausanne, Switzerland
[2]Institute of Geography (GIUB) and Oeschger Center of Climate Change Research (OCCR), University of Bern, Bern, Switzerland.
[3]Department of Environmental Systems Science, ETH Zurich, Zurich, Switzerland
[4]School of Geography, Earth and Environmental Sciences, University of Birmingham, Birmingham, UK
[5]Birmingham Institute for Forest Research (BIFOR), University of Birmingham, Birmingham, UK

Correspondence to: Natalie Ceperley (natalie.ceperley@giub.unibe.ch)

Abstract

Hydrological processes in high-elevation catchments are strongly influenced by snow accumulation and melt and summer rainfall. Diverse water stores and flow paths that generate streamflow in these important water towers emerge from these two driving inputs, but a detailed process understanding remains poor. We measured a combination of natural tracers of water at a high frequency, including stable isotope compositions, electrical conductivity (EC), and water and soil temperature to characterize hydrological processes in a snow-dominated Alpine catchment and to understand the diversity of streamflow sources and flow paths. Stable isotope compositions of the sampled water reveal the prominence of snowmelt year-round (even during winter baseflow) and an strong flushing of the entire system with snowmelt at the start of the main melt period, leading to a reset of the isotopic values in most sampled water. Soil temperature measurements indicate sub-snowpack local flow, for example in the case of rain-on-snow events and help identify snow-free periods. Water temperature measurements in springs can indicate flow path depth. EC measurements further indicate the magnitude of subsurface exchange and allow for the separation of subsurface snowmelt contribution to streamflow from the contribution of stored groundwater. These insights into the details of streamflow generation in such a dynamic environment were only made possible due to the intense, year-round water sampling. The sampled tracers are revealed to complement each other in important ways particularly because they were sampled year-round, specifically during winter and spring, both snow-covered periods, the importance of which is a key implication of this work.

1   Introduction

Hydrology in Alpine environments is largely dominated by snow accumulation and melt processes with ensuing high sensitivity to changes in climate (Hanus et al., 2021). For Alpine catchments with a mean elevation above approximately 1500

masl (Santos et al., 2018), winter snowfall leads to the build-up of a seasonal snowpack, which results in low flow occurring between November and March (Schaefli et al., 2013) and maximum monthly streamflow related to melt between May and August, depending on the depth and extent of the seasonal snowpack and on the degree of glacier cover (Hanus et al., 2021; Muelchi et al., 2021). Given the importance of these cycles of accumulation and melt and the resulting streamflow regime for water resource availability, an important body of literature focuses on quantifying the streamflow regime in such environments, either based on streamflow observations (Blahusiakova et al., 2020; Brunner et al., 2019; Musselman et al., 2021; Hammond and Kampf, 2020) or modelling (Foster et al., 2016; Livneh and Badger, 2020; Muelchi et al., 2021).

Detailed hydrological process studies in high Alpine catchments remain, however, relatively rare even if detailed insights into the fate of rainfall and snowmelt in such catchments are required for model-based extrapolations of their hydrological response into the future, given the likely changes in climate. In addition to logistical challenges, continuous monitoring in frozen environments require development of specific methods and equipment (Rucker et al., 2019), which explains the small number of studies in such places.

Existing field-based studies can be classified according to their focus: i) understanding dominant runoff generation mechanisms during rainfall and snowmelt events (Penna et al., 2016; Engel et al., 2016), including small-scale studies of snowpack flow paths (Webb et al., 2020), ii) understanding the origin of winter low flow (Floriancic et al., 2018), iii) quantification of groundwater or spring recharge (Lucianetti et al., 2020) and seasonal groundwater storage (Arnoux et al., 2020), or iv) understanding the role of glaciers and rock-glaciers in the hydrological response of high elevation catchments (Brighenti et al., 2019; Zuecco et al., 2019; Ohlanders et al., 2013; Penna et al., 2014). A common feature of these studies is the use of natural tracers, such as electric conductivity or stable isotope compositions of water, to gain new insights into the fate of rainfall and snowfall and related water flow paths and to formulate hypotheses about dominant runoff drivers at specific times of the year, or the hydrologic response of selected landscape units.

To help fill some of the important knowledge gaps on elevational and seasonal drivers, this work uses high frequency tracer sampling to quantify drivers of the hydrologic response of a high elevation catchment throughout all streamflow periods, ranging from winter low flow, to different stages of the melt season and the autumn recession by compiling and complementing observational data from the intensively studied Vallon de Nant catchment in the Swiss Alps (Benoit et al., 2018; Giaccone et al., 2019; Ceperley et al., 2020; Mächler et al., 2021; Michelon et al., 2021b; Thornton et al., 2021a; Beria et al., 2020; Antoniazza et al., 2022).

The overall objective of this work is to examine dominant hydrological processes and associated flow paths in Vallon de Nant during different periods of the year through the lenses of four tracers: soil temperature, water temperature, electrical conductivity, and stable isotopes of water. The first tracer used in this study is the stable isotope composition of water, a natural tracer that has been extensively used to characterize snow hydrological processes (e.g. Beria et al., 2018), and is particularly useful to examine the interplay between different water compartments (rainfall, snowpack, springs, groundwater), recharge and evaporation processes (e.g. Sprenger et al., 2016). Electrical conductivity measurements as an additional tracer provides information on subsurface flow paths and water residence times in the subsurface (Cano-Paoli et al., 2019). Water temperature

measurements can be used to quantify connectivity between water sources and the atmosphere (Constantz, 2008). And lastly, soil temperature measurements are used to identify periods of thermal insulation from the seasonal snow cover (Trask et al., 2020).

70 Using these tracers, we explore the origin of winter streamflow (from groundwater or from localized snow melt) (Floriancic et al., 2018; Hayashi, 2020), the dominant runoff processes that drive streamflow generation during early compared to late snow melt phase (Brauchli et al., 2017) and during the seasonal recession, the streamflow generated by shallow groundwater in the hillslopes and of alluvial or talus groundwater systems throughout the year (Hayashi, 2020). These explorations provide key transferable insights into the value of these four tracers for hydrologic process investigation that are relevant for 75 comparable catchments.

2 Data and Methods

2.1 Study area

The following case study description is largely based on the paper by Michelon et al. (2021b). Vallon de Nant is a 13.4 km² headwater catchment located in the western Swiss Alps (Figure 1), with elevation ranging from 1200 to 3051 masl (mean 2012 80 masl). The catchment has an elongated shape and runs from south to north, along the river Avançon de Nant.

The Vallon de Nant is of national importance in Switzerland for its biodiversity (Cherix and Vittoz, 2009) and has been protected since 1969 (Natural Reserve of the Muveran). The site has been the focus of a number of recent research projects, in disciplines such as hydrology (Michelon et al., 2021b; Beria, 2020), hydrogeology (Thornton et al., 2021a), pedology (Rowley et al., 2018) biogeochemical cycling (Grand et al., 2016), geomorphology (Lane et al., 2016) and vegetation ecology (Vittoz, 85 2012; Giaccone et al., 2019), as well as interactions between biology and hydrology (Mächler et al., 2021) and stream ecology (Horgby et al., 2019).

The catchment lies on the backside of the Morcles nappe (Huggenberger, 1985). The Cretaceous and Tertiary lithologies are organized as a succession of thick, blocky layers exposed throughout the surrounding valley. They rest on a substratum of flysch, i.e. softer rocks (schistose marls and sandstone benches), which explains the deepening and widening of the valley at 90 its southern part (Badoux, 1991).

In the southern part of the valley, there is a glacier (Glacier des Martinets), with a surface of 0.58 km² in 2016 (Linsbauer et al., 2021) at relatively low elevation (2126 to 2685 masl) lying on the northern, shady side of the Dent de Morcles. Due to its small size, its high debris cover and low radiation exposure, the glacier is likely to have a small contribution to the catchment-scale streamflow (Mächler et al., 2021). The water flow paths through and below the debris-covered glacier are unknown to 95 date and are not specifically investigated as part of the present research.

The eastern side of the catchment is marked by steep and rocky slopes associated with thin soils and debris cones at the foot of the rock walls in the north-eastern part. Along the rock walls, all lateral tributaries are ephemeral, flowing principally during the snowmelt season or shortly after the rainfall events; their extent fluctuates and is not known precisely.

The western side of the valley is associated with grassy slopes, relatively well-developed soils, and hence relatively high water-storage capacities (see pictures, Figure S1). The valley has had a relatively stable vegetation cover, composed of grassland and spruce (based on a comparison of historical with recent photographs, see Figure S2 in Supplementary Material). The distribution of stands of spruce (Dutoit, 1983), which are intermixed with corridors of scrub vegetation on the north-western slopes, are controlled by regular avalanches. Above the spruce stands, there is a transition band to subalpine and high elevation vegetation, consisting of intermixed larch, pasture, and alder.

The location of springs correlates with low slopes (see Figures S4 and S6 in Supplementary material), a topographic particularity explaining the location of springs along the right bank of the main stream and within the grassy slopes in the western area of the catchment, where the slopes are low. In the same way, the absence of tributaries over the north-western parts of the catchment are related to steep slopes, explained by the large hydraulic conductivity and locally well-developed soils. The high water-storage capacity of the well-developed soil is also indicated by salt gauging along the main stream during the late summer and autumn streamflow recession period in 2016 and 2017 (see Figure S5 in Supplementary Material).

The riparian wetland (Figure 1), at least in its southern part, is made of coarse and permeable alluvial sediments associated with a high hydraulic conductivity; it could be "hydrologically active" to its full depth, which can exceed 80 m (Thornton, 2020). The extent of the stream network is based on observations during dry and wet periods (Michelon et al., 2021b) and its exact path is calculated using the Swiss digital elevation model at a resolution of 2 m (Swissalti3d, 2012). During wet periods, the stream network (as shown in Figure 1) extended to 6 km; during dry periods, the main stream contracted to as short as 2.95 km, corresponding to the channelized flow starting at 1480 masl. During the period of snow accumulation, the stream network extent was difficult to establish but there was no known occurrence of zero flow.
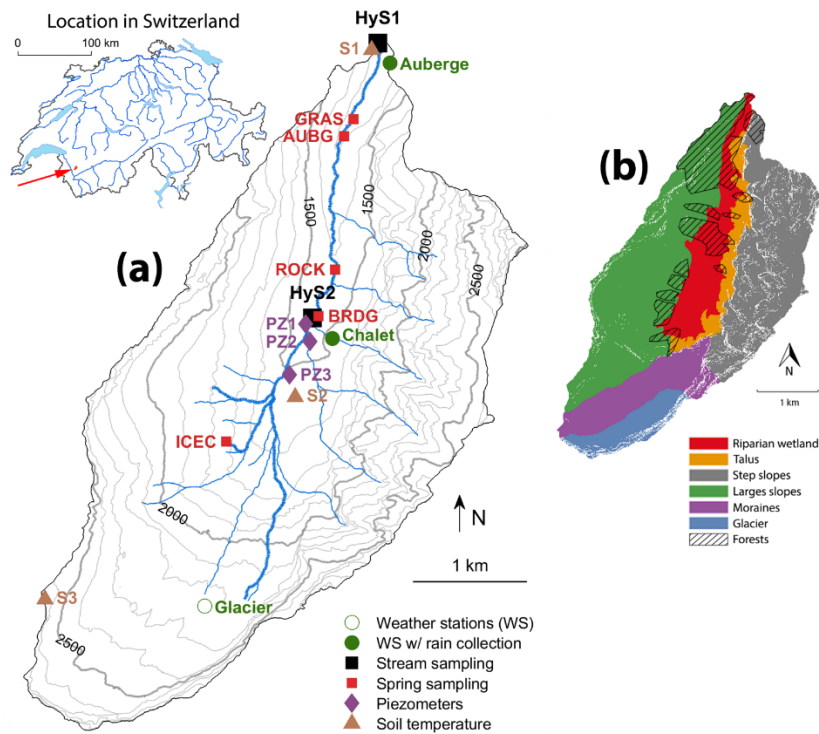
Figure 1. The map A), based on the 2m digital elevation model (Swissalti3d, 2012) shows the location of the sampling sites in the Vallon de Nant (outlet at 46.25301°N, 7.10954°E in WGS84, elevation 1200 masl). The list of locations is given in the Supplementary Material, Table S1. The stream network shows the full extent, which is only during snowmelt periods. The AUBG spring location shows where the water is sourced from, even though it is sampled from a pipe at the Auberge weather station point, 800 m further north. The map B) identifies the dominant hydrological units of the Vallon de Nant and the hatched area corresponds to forested areas.

2.2   Meteorological and hydrological data

Meteorological variables are monitored at three locations (Michelon et al., 2021a) along a north/south transect (at 1253 masl, 1530 masl and 2136 masl) since September 2016 (see Figure 1). The precipitation intensity is measured using a 24 GHz Doppler radar sensor (Lufft WS400-UMB, G. Lufft Mess- und Regeltechnik GmbH, Fellbach, Switzerland) that distinguishes the precipitation phase (rain and snow), available from Michelon et al., (2021a). We have access to piezometric data from the work of Thorton et al., (2021) at two locations in the alluvial flood plain (Figure 1) to characterize the dynamics of the corresponding ground water system. The streamflow at the catchment outlet (HyS1, Figure 1) is monitored since September 2015 via river height measurements using an optical height gauge (VEGAPULS WL-61 optical height gauge, VEGA, Schiltach, Germany, see photo in Figure S3) above the middle point of a trapezoid shape weir. It averages water height every minute continuously. The height is then converted into streamflow using a rating curve based on 55 salt gauging of discharge (Ceperley et al., 2018). The rating curve relating height to discharge is a power-relationship using the nonlinear least squares

method (The Mathworks, 2017) with the trust region algorithm and least absolute residual method to obtain a 95% confidence interval. To guide the analysis of the streamflow response throughout the year, we analyzed in detail the different streamflow periods (Section **Error! Reference source not found.**) based on the 7-day moving average streamflow data (Q_{m7}) and the daily change of Q_{m7}, called ΔQ_{m7}.

2.3 Stable isotopes of water

2.3.1 Water sampling

Water (from streams, springs, and piezometers) was either sampled manually (grab samples) or via automatic samplers placed at the outlet and an upstream location along the stream (HyS1 and HyS2; Figure 1) for stable isotope analysis (δ^2H, $\delta^{17}O$ and $\delta^{18}O$). A three- or four-letter code was adopted for all sampling locations that is visible on the map (Piezometers: PZ1, PZ2, PZ3; Springs: GRAS, AUBG, ROCK, BRDG, ICEC; and Stream: HyS1, HyS2; Figure 1). Twelve mL amber borosilicate glass vials with polypropylene screw-top caps with PTFE-lined silicone septa were used for all sample transport and storage. When possible, samples were stored sealed in a refrigerator (~ 4°C) until analysis but in some cases were stored at ambient temperatures. In all cases, they were kept out of direct light and heating. Automatic sampling was performed with an ISCO 6712C Compact Portable Sampler with 24 bottles of 500 mL capacity at HyS1 and an ISCO 6712 full-size portable sampler with 24 bottles of 1L capacity at HyS2 (Lincoln, Nebraska, USA). Automatic samplers were programmed to sample at 6-hour intervals over one week. The automatic sampler was programmed to fill bottles to half of their capacity, 250 mL and 500 mL, respectively, to optimize energy usage and to prevent sample loss due to freezing, while still sampling enough water to limit fractionation due to evaporation.

A sub-sample of water was then taken manually from each bottle either in the laboratory or in the field. Original installation involved the use of pipettes and tubes inside the autosampler bottles similar to those described by Von Freyberg et al. (2020), however after some experimentation and due to the Alpine and shaded microclimate of the location, fractionation due to evaporation was deemed minimal and additional components resulted in more contamination and less sampling capacity. In case of freezing, the bottles were closed with a cap and moved to a warmer place until the ice fully melted.

Samples of rainfall were collected at the *Auberge* and *Chalet* meteorological stations (Figure 1) with a 13 cm diameter plastic funnel, connected to an insulated 2.5 L screw-top bag made of 147 μm PET/NY/LDPE plastic (DaklaPack, Perpignan, France), enclosed in a plastic box. The collected water was well mixed, weighed and sub-sampled once or twice a week from May to November (outside the snowfall period).

Groundwater was sampled from piezometers (Thornton et al., 2021a). Prior to water sampling, the piezometers were emptied using a Geotech Peristaltic Pump (Geotech Environmental Equipment, Inc, Denver, Colorado, U.S.A.); and the freshly recharged water was sampled with the same pump and stored in 12 mL amber glass vials.

During winter 2017 and winter 2018, snow samples were collected regularly at two locations. Two different sampling methods were used: i) if distinguishable snow layers were present (visual and textural distinction) each of them was sampled individually, otherwise ii) a single bulk sample of approximately sampled the entire profile was taken.

Snow was sealed in alimentary 700 mL zip bags made of 120 μm BOPP/LPDE plastic (DaklaPack, Perpignan, France) after evacuating as much air as possible. The collected snow samples were melted at ambient air temperature (the influence of water vapor from air on the isotopic composition of the sample is discussed in the Appendix 1). A sub-sample of well-mixed, melted snow was taken manually in the lab from each bag.

The isotopic composition of the entire snowpack at a given snow pit was obtained with a weighted average of the values of each sampled layer according to depth, as an approximation for the equivalent bulk isotope composition assuming a uniform density.

2.3.2 Analysis of the isotopic composition of water

Stable isotope compositions of water, expressed using the familiar δ notation (δ^2H, $\delta^{17}O$ and $\delta^{18}O$), were measured with a Picarro 2140-i Wavelength-Scanned Cavity Ring Down Spectrometer (Picarro Inc., Santa Clara, California, U.S.A.), using 2.0 mL glass vials closed with screw-top caps with silicone Rubber/TPFE septa and filled with 1.8 mL of filtered water. Samples were injected between 6 and 8 times (Penna et al., 2012). The first 3 injections were discarded to avoid memory effects (Penna et al., 2012). The raw values were then corrected according to a standard curve determined with 3 internal standards, which are regularly calibrated against the international standards of VSMOW (Vienna Standard Mean Ocean Water) and SLAP (Standard Light Antarctic Precipitation) of the IAEA (International Atomic Energy Agency)(Coplen, 1994). Each standard was injected 12 to 15 times, and data from the final 6 injections were kept. Delta units of isotope compositions (Coplen, 1994) are reported in per mil and the strategy used for the analysis is similar to the one described in the work of Schauer et al. (2016). The median analytical errors obtained with this method are 0.4 ‰ for δ^2H, 0.01 ‰ for $\delta^{17}O$, 0.04 ‰ for $\delta^{18}O$.

Based on these measures, we compute d-excess (Dansgaard, 1964) and ^{17}O-excess (Barkan and Luz, 2005; Landais et al., 2006):

$$\text{d-excess:} = \delta^2H - 8 \cdot \delta^{18}O, \tag{1}$$

$$^{17}O\text{-excess:} = 10^6 \left(ln\left(\frac{\delta^{17}O}{1000} + 1\right) - \lambda_{ref} \cdot ln\left(\frac{\delta^{18}O}{1000} + 1\right) \right), \tag{2}$$

with λ_{ref} = 0.528 (Meijer and Li, 1998; Barkan and Luz, 2005; Landais et al., 2008). From regression of $ln(\delta^{17}O/1000 + 1)$ against $ln(\delta^{18}O/1000 + 1)$, we obtain a similar slope for our samples (λ_{ref} = 0.528), which confirms the universality of this value. However, memory effects can notably influence the $\delta^{17}O$ measurements in cases of larger variations in values within any one sequence measured (Vallet-Coulomb et al., 2021).

To gain insights into local evaporative processes, we compute the line-conditioned excess lc-excess (Landwehr and Coplen, 2006) based on our local meteoric water line LMWL :

200   lc-excess: $= \delta^2 H - a \cdot \delta^{18} O - b.$ (3)

2.3.3   Isotopic lapse rate estimation

We estimate elevation gradients of isotopic ratios, i.e. lapse rates, based on the median of measurements at different locations for precipitation and streamflow. For precipitation, we use the measurements at Auberge station (elevation 1253 masl) and Chalet station (elevation 1517 masl). For streamflow, we use the measurements of station HyS1 (elevation 1248 masl) and
205   HyS2 (elevation 1469 masl). For other sampled waters, we do not establish lapse rates due to varying number of samples and inconsistent sampling dates.

2.4   Water temperature and conductivity measures

The water temperature of four springs was recorded every 30 minutes (every 15 minutes for GRAS and ROCK springs) with Hobo temperature loggers (Onset Computer Corporation, Bourne, MA, U.S.A.) for periods between 12 and 21 months. Based
210   on these recordings, we estimate lag times with respect to air temperature and diel and annual amplitudes. The original time resolution of 1 minute for the stream, 30 minutes for piezometers (PZ) and 2 minutes for springs is kept for the diel temperature maximum amplitude but aggregated to 1 day for the annual temperature maximum amplitude (using a 7-day moving average, see Figure S9). Lag times are obtained by maximizing cross correlation between the 1-day signal and the one for the reference air temperature signal (Figure 1, Auberge station). Electrical conductivity (EC) was measured for all collected water samples
215   except snowpack, either directly in the field with a WTW Multi 3510 IDS connected to a WTW TetraCon 925 probe (Xylem Analytics Germany Sales GmbH & Co, Weilheim, Germany) or in the laboratory directly in the vials using a JENWAY 4510 Conductivity Meter with a 6 mm glass probe (Stone, U.K.). Comparison of duplicate measurements using both probes (compensated in temperature) demonstrated a correlation coefficient of $R^2=0.89$ despite a delay of 23 to 30 months between the in situ and laboratory measurements (see Figure S7 in Supplementary Material).
220   Water temperature was analyzed with a simple analytical temperature model with sinusoidal initial conditions (e.g. Elias et al., 2004) to compute a rough depth that would correspond to such a lag L (for details see Appendix 2). For example, assuming a typical thermal diffusivity of soil of $5.56 \ 10^{-7}$ m^2/s (Elias et al., 2004) a lag of 41 days would correspond to a depth of 1.7 m, a lag of 39 days to 1.6 m.

2.5   Soil Temperature measures

225   The soil temperature at three different elevations (at 1240 m, 1530 m, and 2640 masl, see Figure 1) was monitored from July 2009 to November 2018 using GeoPrecision M-Log5W (GeoPrecision GmbH, Ettlingen, Germany) at 10 cm depth (see Figure 1) and recorded hourly (Vittoz, 2021) . Soil temperature is a good proxy for snow cover, making distributed observations particularly useful. Strong diel variations of can be associated with snow-free soils, which correlate with the larger amplitude air temperature fluctuations and radiative exchanges.

230

3 Results

3.1 Streamflow response characterization

The annual average streamflow over 2017 and 2019 was between 0.46 to 0.62 m^3 s^{-1} (3.0 to 4.0 mm d^{-1}) but fluctuated between 0.02 to 0.03 m^3 s^{-1} (0.12 to 0.18 mm d^{-1}) and 2.4 to 3.1 m^3 s^{-1} (15.5 to 19.7 mm d^{-1}). Peak monthly flow occurred either in June (for 2017-2018 and 2018-2019) or July (2016-2017, the year with abundant winter snow). Flood events resulted in streamflow peaks as high as 5.8 m^3 s^{-1} and up to 7.2 m^3 s^{-1} (37.4 to 46.3 mm d^{-1}) over 1 hour and from 6.9 to 8.5 m^3 s^{-1} (44.4 to 54.6 mm d^{-1}) over 10 minutes. The mean temperature of the streamflow at the outlet (1200 masl) was 5.0 °C and ranged from 0 °C when the river was frozen during some winter periods to a daily temperature of 10.0 °C during summer. As a comparison, the annual mean air temperature at mean elevation (2012 masl) was 3.1 °C in 2017 (considerable data gaps in 2018), based on data from 3 stations (Glacier, Auberge, Chalet; Fig. 1).

Based on the moving average streamflow Q_{m7} and the corresponding daily fluctuations ΔQ_{m7}, we identified four characteristic streamflow periods (Figure 3): baseflow (B), early melt (E), melt (M) and recession (R). The two main features of these periods are: i) streamflow increase during E and M and decrease during R and B and ii) a range of daily values that is very low for B (around 0.02 m^3/s), relatively low for E and R (0.1 m^3/s) and considerably higher for M (0.3 m^3/s).

Period B extended from the end of September to early spring (between mid-March and beginning of April), when the streamflow was approximately 1 mm d^{-1}, which is typical for catchments at comparable elevations (Floriancic et al., 2018). The baseflow exhibited a very slow decrease across the period B, with almost no diel variations even though some streamflow peaks occur due to exceptional rainfall events or warm periods (e.g. January 2018). B had Q_{m7} values lower than the 30th percentile of observed streamflow.

During E, streamflow started increasing to a few mm d^{-1}, preceding the main snow melt period M, but the daily range did not show a large increase. E lasted up to several weeks in certain years (e.g. in 2017) and was absent in one year (2018), when warming occurred extremely quickly. E had Q_{m7} values around the 50th percentile. The average ΔQ_{m7} is 0.64 mm per day (0.1 m^3/s). M corresponds to the period with important water inputs from snowmelt. Compared to E, there is a much higher diel variation in streamflow (resulting from diel snowmelt patterns). In 2017, M started at the beginning of May and at least a month earlier in 2018. M has Q_{m7} values above the 80th percentile. The average ΔQ_{m7} is greater than 0.64 mm per day (0.1 m^3/s). The time of diel peak discharge (in absence of rainfall input) is between mid-day or late afternoon.

R was set to begin after the annual maximum of average Q_{m7}, which for 2016 was end of June (preceded by a very snow-rich winter), for 2017 end of May and for 2018 to beginning of June. R results from a combination of reduced input from snowmelt and evaporation, as clearly visible in the significant diel streamflow variations during R. Q_{m7} values were around the 70 to 75th percentiles. and ΔQ_{m7} was close to -0.64 mm per day (-0.1 m^3/s). The time of diel peak streamflow was in the morning or early afternoon. A summary of streamflow characteristics during all four periods is included in Table S2.
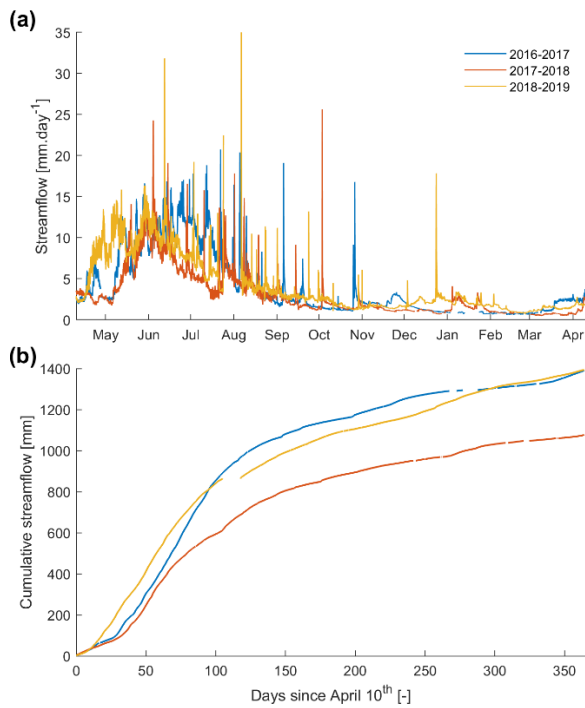
Figure 2. Comparison of the streamflow evolution (a) and cumulation (b) per year for 3 years. The start is here 10 April of each year, which corresponds to the start of the earliest start of the early melt period E (Section **Error! Reference source not found.**). There are gaps in the data, 6.4%, 3.2% and 4.6% of the time series are missing (respectively in 2016-2017, 2017-2018 and 2018-2019).

3.2   Soil temperature

3.2.1   Soil temperature dynamics

The fluctuations in soil temperature at three different elevations (1240 m, 1530 m, and 2640 masl) revealed seasonal, daily, and spatial variation (Figure 3). As winter approached each year, soil temperature gradually dropped towards, but did not reach 0 °C. The slightly positive temperature can likely be explained by ground heat flux. Once snow fell, the insulation its cover provided is visible as a dampened diel temperature variation that is less correlated with daily air temperature fluctuations than in snow free periods. Some isolated temperature spikes are observed during winter, probably due to rain-on-snow events (e.g. the spike during winter 2016 in the green line in Figure 3, at the lowest elevation) that were visible in the temperature signal but apparently did not generate any streamflow. Unfortunately, no other observed tracers are available during these periods to confirm this hypothesis.

The negative temperatures measured during the 2016-2017 winter period by two soil temperature probes (at 1530 m and 2640 masl) can be explained by the cold air temperature and the exceptionally dry winter with a low snow cover (see a detailed discussion of soil temperature recordings under snow cover in the work of Bender et al., 2020). The variation in temperature at the three different elevations in Figure 3 displays the elevation gradient that alters the start of the snow-free period at the

different elevations, and the elevation-dependency of the timing of strong warming (of more than 5 °C) between March and July. The start of the snow-free period occurred between 4 (2018) and 8 weeks (2017) earlier at 1240 masl elevation than at 1530 masl, whereas between 1530 masl and 2640 masl, it was delayed by between 3.5 (2018) and 8 weeks (2016).

285   Similarly, the soil temperature time series clearly showed the elevation dependency of the arrival of snow. It arrived much earlier (12 weeks) in autumn 2016 at the highest elevation as compared to the two lower elevations. In 2017, the seasonal snow cover onset occurred at a similar time at all elevations, as we see that all diel temperature variation disappears between October 22nd and November 25th. A summary of snow-free dates as extracted from the temperature recordings is available in the Supplementary Material (Table S3).
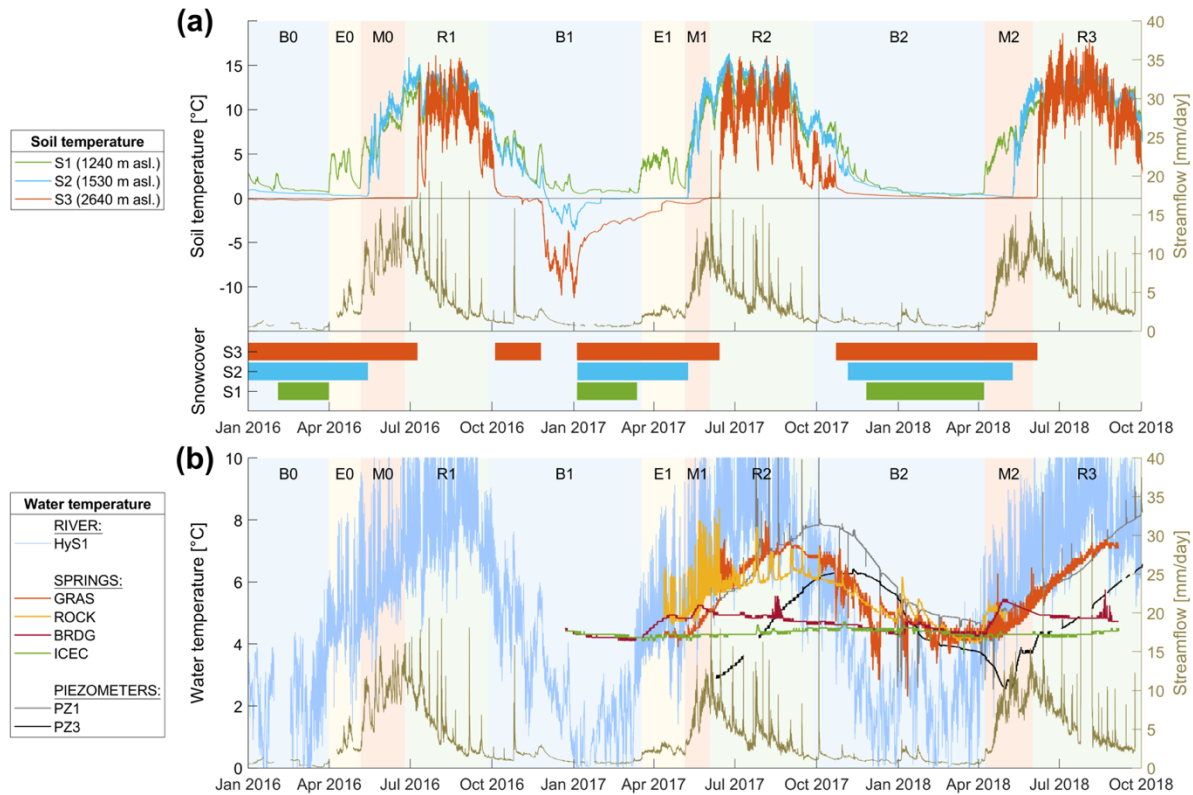
290

Figure 3. Evolution of soil temperature (a) at 3 locations within the Vallon de Nant catchment (S1, S2, S3) and (b) of the stream at the outlet (HyS1), 4 springs (GRAS, ROCK, BRDG, ICEC) and groundwater at 2 locations (PZ1, PZ3) between January 2016 and October 2018. A summary of dates corresponding to the 11 runoff periods divided by baseflow (B0, B1, B2), early melt (E0, E1), melt (M0, M1, M2), and recession (R1, R2, R3) is available in the Supplementary Material (Table S2).

3.2.2 Soil temperature links to streamflow

Interesting features can be observed when soil temperature is examined with respect to the identified streamflow periods. For all three melt periods (M), soil temperature recordings from the highest elevation showed the presence of snow until the start of the recession period (R), which demonstrates the late melt of seasonal snow in some areas of this catchment. The start of the two early melt periods (E) in 2016 and 2017 corresponded to the disappearance of snow at the lowest soil temperature measurement point (1230 masl).

Decline in soil temperature started at a similar time across all elevations and corresponded closely with the start of the streamflow Baseflow periods (B), or in other words, the significant decrease in soil temperature only started when the streamflow recession period (R) was already advanced. In the winter of 2016/2017, winter streamflow fluctuations were reflected in soil temperature, whereas the mid-winter streamflow rise in January 2018 was not visible in any of the soil temperature recordings, however this may be due to errors in recording river stage caused e.g., by accumulated sediment (Michelon, 2022, chapter 3).

Finally, from the covariation between soil temperature and streamflow, we can deduce that during M, runoff-generating rainfall events coincide with cold spells, whereas during autumn, runoff-generating rainfall events coincide with warm spells (e.g. October 2016 and 2017).

3.3 Water temperature

3.3.1 Influence of air temperature on stream temperature

Average recorded stream temperature at the outlet was 5.0 °C, which is slightly higher than 3.1 °C, the average recorded air temperature at mean elevation 2012 masl. The fluctuation of water temperature at the catchment outlet (HyS1, Figure 1) are correlated with the variations of the air temperature ($R^2 = 0.87$) at the Auberge weather station and the annual cycle shows no lag between them. The close correspondence can be explained by the fact that the in-stream travel time is long enough for atmospheric heat exchange to exert a strong influence on water temperature (Gallice et al., 2015). The importance of instream atmospheric heat exchange can also explain the high annual and diel temperature amplitudes (**Error! Reference source not found.**), which corresponded closely to the observed air temperature amplitudes over the year (between 17.5 and 19.5 °C at the lower elevations, with a 30-day moving average).

3.3.2 Groundwater temperature patterns in springs and piezometers

Observation of patterns in the temperature of springs and groundwater reveal hints of underlying flow generation processes. Indicators of these processes include correlation between water and air temperature, diel temperature variations, temperature response to rainfall events, the overall pattern and shape of temperature fluctuations on a seasonal scale, mean values and convergence between different points over the study area, and temperature anomalies and their timing. First, we observe that the correlation between water temperature in springs and in piezometers and air temperature, measured at the Auberge station,

varied by location (**Error! Reference source not found.**); PZ1 correlated the strongest (R^2=0.80) and ICEC the least

330   (R^2=0.56), and none as strongly as the surface water (R^2 = 0.87, described above).

In general, diel temperature variations were rare and can probably be explained by poor measurement when water volume was low. The temperature in some springs reacted to precipitation while that in others did not. The GRAS spring had a permanent but small outflow of only a few liters per minute (personal observation). Since the temperature was recorded directly in the outflowing water, the sensor might have been heated up by atmospheric heat exchange when outflow was low. This most

335   probably explains some strong sub-diel temperature fluctuations of the GRAS (and ROCK) springs (Figure 3). Despite these diel fluctuations, the GRAS temperature signal did not react to summer rainfall events (visible as peaks on the streamflow), whereas ROCK reacted.

The shape of the curve of temperature fluctuations gives us clues to the flow that fed the springs. For example, that of the BRDG spring differed from the sinusoidal shape of the GRAS and ROCK springs, which match the air temperature variations

340   more closely. The BRDG spring signal showed a constant temperature during winter, with an increase during E and M, when it rose from 4.3°C to 5.4°C over 3 weeks at the beginning of M2. The temperature stopped rising around when the soil temperature at mid-elevation indicated snow disappearance (blue bar in Figure 3) and then receded to winter base temperature. By combining the observation of a strong reaction during melt at low elevations with the return to a base temperature during winter, we can deduce that BRDG spring is fed by snowmelt from low elevations (from the right bank riparian area where it

345   is located) during spring and by groundwater the rest of the year.

All spring temperatures converged to around 4.3 °C at the end of B2 (the only winter period measured in all springs), which corresponds to the almost constant temperature of ICEC spring (annual amplitude of 0.4 °C, **Error! Reference source not found.**). This may indicate that at this point in the year, all springs are fed by a common or similar ground water source with little influence of intermediary subsurface or surface flows.

350   The two piezometers that access the groundwater (PZ1 and PZ3) are in the alluvial floodplain across which the stream meanders into an alluvial plane. During intense rainfall events, PZ1 shows strong positive temperature excursions, which even exceeded the temperature of the main channel in summer, however its winter anomalies were less extreme. The annual cycle of the PZ1 temperature reached its maximum temperature of 7.9 °C with a delay of 74 days (2.5 months) after the air maximum and exceeded the maximum recorded in the springs by 1.5 °C. The strong delay of the annual cycle together with the warm

355   temperatures and relatively small amplitude dampening compared to ROCK and GRAS springs suggests that it is influenced by a large storage volume which induces the delay and is closely connected to heat input from the surface.

PZ3 shows the same annual temperature amplitude as PZ1 but has an even longer delay (21 days with respect to PZ1) and has a negative offset of 1.5 °C of its maxima (6.4 °C for PZ3) compared to PZ1, possibly related to the higher elevation and more northern aspect of its source area (PZ3 is located 30 m higher, in the more north-facing part of the catchment). PZ3 has,

360   however an average temperature of 4.8 °C closer to the one of the springs.

A distinctive feature of PZ3 is its temperature decrease during M2, in phase (but in opposite direction) with the streamflow increase. This suggests a direct, relatively important cold input during snow melt, resulting from a high hydrologic connectivity

of PZ3 to snowmelt water (either directly or via exfiltration from the stream) and a low storage volume during this time of the year.

3.3.3 Flow path depth estimation from temperature measures

Dampening depths estimated with the simple temperature model (Appendix 2) from groundwater temperature patterns ranged between 1.2 and 5.4 meters (**Error! Reference source not found.**) and the lag in temperature for those same points compared with streamflow ranged from 41 to 133 days. We attribute these values to the delay resulting from heat conduction (depending on the soil's thermal diffusivity D) and advection with water flow. The one exception is BRDG, for which lag estimation fails, perhaps indicating that this spring is not truly groundwater fed. These lag values are furthermore coherent with the dampening: stronger lags correspond to stronger dampening and are associated with deeper depths. They should however be interpreted with care as i) the presence of an insulating snowpack on the hillslopes prevents heat advection during winter in a similar way that soil would, thereby further contributing to temperature lags and amplitude dampening in the subsurface, and ii) the model is only based on heat conduction and does not account for advection that could be locally important, particularly during snowmelt inputs.

The BRDG spring highlights these limitations, as the temperature variation over the year (0.9 °C) happens over few weeks during the melt periods (M1 and M2). This variation shows a strong reactivity to the snowmelt input but the resulting estimation of flow path depth (0.2 m) is obviously erroneous. At this time, the maximum air temperature is not reached yet (during R2 and R3) and the expected heat signal transferred from air by conduction later in the year is not visible.

Table 1. Statistics of temperature time series recorded in the stream, piezometers, and springs. The dampening depth estimated for the BRDG spring (*) is biased because of a positive anomaly of temperature due to snowmelt input (see text).

Water source	Mean T [°C]	Max T [°C]	Annual T amplitude [°C]	Max. diel T amplitude [°C]	Cross corr. w/ air T Lag [days]	Max corr. [-]	Dampening depth [m]	Snowmelt anomaly	Rainfall anomaly
Stream	5.0	13.4	8.8	11.4	0	0.92	-	-	-
PZ1	6.3	7.8	3.8	4.0 (punctually)	79	0.80	3.2	No	Yes
PZ3	4.8	6.3	3.7	0.5 (punctually)	105	0.68	4.3	Negative	No
GRAS	5.5	7.4	3.0	2.4	41	0.76	1.7	No	Yes
ROCK	5.4	6.7	2.5	2.9	39	0.76	1.6	Positive	yes
BRDG	4.7	5.6	0.9	0.9	6	0.68	0.2*	Positive	No
ICEC	4.3	4.7	0.4	0.6 (noise)	133	0.54	5.4	No	No

3.4   Electrical conductivity

The range of conductivity for stream, springs, groundwater, rainfall, snowpack, glacier and vegetation water samples is shown in Figure 4.   The Figure 4. Range of δ^2H, $\delta^{17}O$, $\delta^{18}O$, conductivity, d-excess, lc-excess and ^{17}O-excess for stream, springs, groundwater, rainfall, snowpack, glacier and vegetation water samples. For measurements of the same water type (STREAM, SPRINGS, RAIN), the lowest sampling elevation is given on top, the highest on the bottom. The left and right end of each box show the 25th and 75th percentiles, and the middle point is the median. The whiskers go up to 1.5 times the interquartile range; values beyond the whiskers (outliers) are marked with circles. The values on the right y-axis of the figures are the number of samples in each category. Note that there are no conductivity measurements for snowpack and vegetation water samples. For ^{17}O-excess the values of vegetations samples are out of the box (median 572 ‰, 25th and 75th percentiles are 374 ‰ and 742‰, resp., and whiskers are from 31 ‰ to 8329 ‰).time series of conductivity for 5 springs is shown in Figure 5, at the outlet HyS1 and at the upper subcatchment outlet, HyS2, in Figure 6, and for rainfall (from Auberge and Chalet weather stations) in Figure 7.

The median electrical conductivity of 216 µS/cm in streamflow at the outlet is relatively high for alpine environments. The electrical conductivity observed at the outlet and in the upper subcatchment (HyS2, median EC of 215 µS/cm) were very close. Assuming a spatial homogeneity between flow path depth and flow velocity, their proximity suggests a similar flow path length distribution. The temporal evolution of stream EC included a decrease in EC during the melt season. A time lag between seasonal cycles in EC and streamflow cycles is seen in Figure 6. This event-scale lag accumulates into a shift of the seasonal cycle in streamflow and EC.

All springs, except ICEC had higher EC values than the stream or the directly sampled groundwater. Higher EC values point towards longer flow paths in the subsurface, either vertically or laterally (Cano-Paoli et al., 2019), or alternatively longer residence times of the water, hence lower flow rates. The spring with the highest EC (GRAS, median EC of 271 µS/cm) showed the least temperature dampening, and the spring with the lowest EC (ICEC, median 211 µS/cm) shows the most dampening (where high amounts of dampening indicates deep flow paths in the subsurface). Assuming a homogeneous underlying geology, the only possible explanation of EC signals in conjunction with the temperature signals is that low EC values of subsurface water result from short flow paths in the shallow subsurface (GRAS spring), and relatively high EC values result from longer and deep flow paths (ICEC).
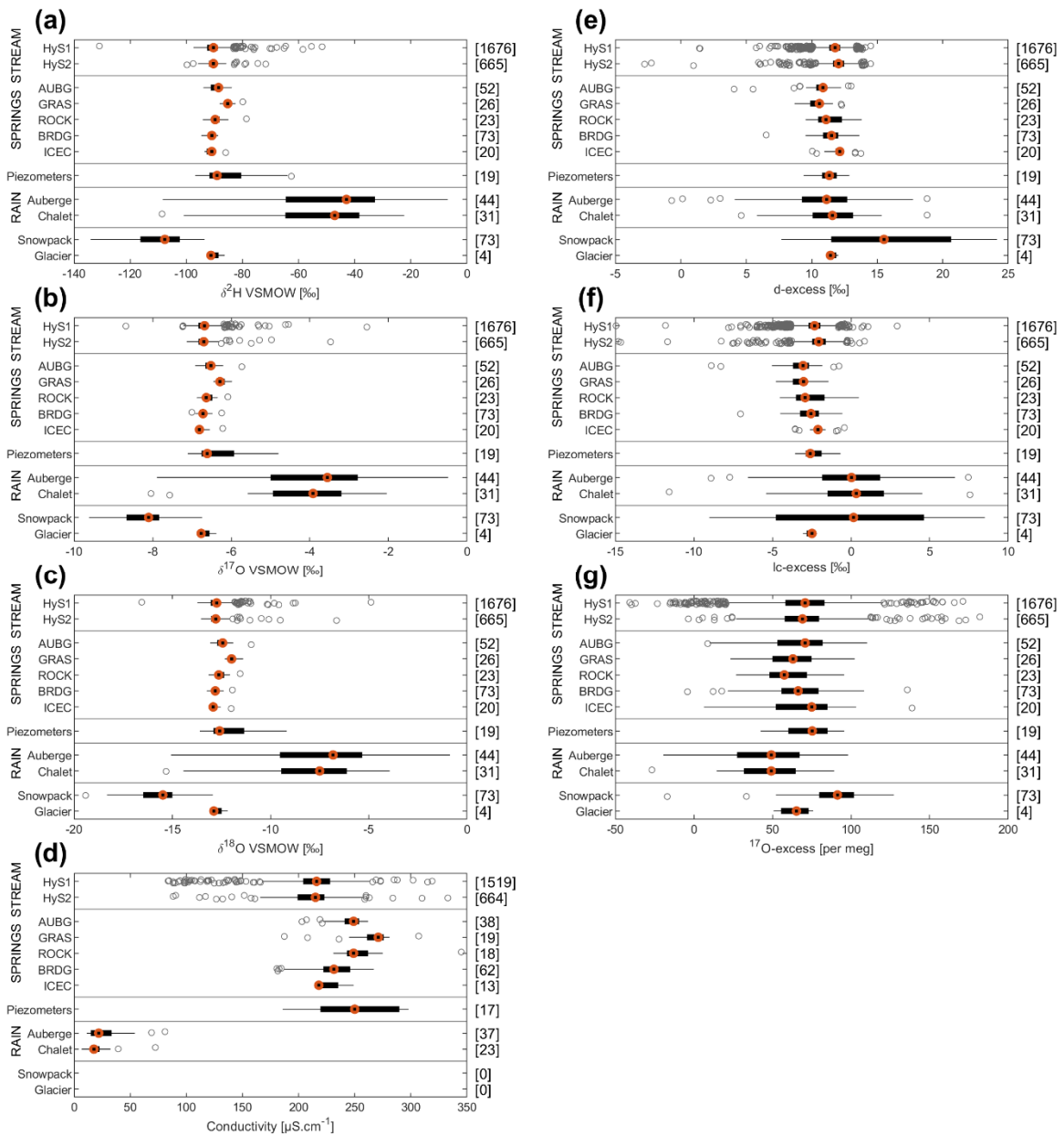
410

Figure 4. Range of δ^2H, $\delta^{17}O$, $\delta^{18}O$, conductivity, d-excess, lc-excess and ^{17}O-excess for stream, springs, groundwater, rainfall, snowpack, glacier and vegetation water samples. For measurements of the same water type (STREAM, SPRINGS, RAIN), the lowest sampling elevation is given on top, the highest on the bottom. The left and right end of each box show the 25th and 75th percentiles, and the middle point is the median. The whiskers go up to 1.5 times the interquartile range; values beyond the whiskers (outliers) are marked with circles.

415   The values on the right y-axis of the figures are the number of samples in each category. Note that there are no conductivity measurements for snowpack and vegetation water samples. For ^{17}O-excess the values of vegetations samples are out of the box (median 572 ‰, 25th and 75th percentiles are 374 ‰ and 742‰, resp., and whiskers are from 31 ‰ to 8329 ‰).

3.5   Stable isotope compositions of water

The range of δ^2H, $\delta^{17}O$, $\delta^{18}O$, d-excess, lc-excess and ^{17}O-excess for stream, springs, groundwater, rainfall, snowpack, glacier and vegetation water samples is shown in Figure 4. The Figure 4. Range of δ^2H, $\delta^{17}O$, $\delta^{18}O$, conductivity, d-excess, lc-excess and ^{17}O-excess for stream, springs, groundwater, rainfall, snowpack, glacier and vegetation water samples. For measurements of the same water type (STREAM, SPRINGS, RAIN), the lowest sampling elevation is given on top, the highest on the bottom. The left and right end of each box show the 25th and 75th percentiles, and the middle point is the median. The whiskers go up to 1.5 times the interquartile range; values beyond the whiskers (outliers) are marked with circles. The values on the right y-axis of the figures are the number of samples in each category. Note that there are no conductivity measurements for snowpack and vegetation water samples. For ^{17}O-excess the values of vegetations samples are out of the box (median 572 ‰, 25th and 75th percentiles are 374 ‰ and 742‰, resp., and whiskers are from 31 ‰ to 8329 ‰).time series of $\delta^{18}O$, $\delta^{17}O$, d-excess, lc-excess and ^{17}O-excess for 5 springs is shown in Figure 5, at the outlet HyS1 and at the upper subcatchment outlet, HyS2, in Figure 6, and for rainfall (from Auberge and Chalet weather stations) and snowpack in Figure 6. Additional figures displaying further variables (i.e. δ^2H) are in the Supplement (Figure S10).

3.5.1   Ranges and lapse rates of δ^2H, $\delta^{17}O$ and $\delta^{18}O$

The median $\delta^{18}O$ value of all streamflow samples was -12.7 ‰. An isotopic lapse rate of 0.84 ‰/100 m for δ^2H and 0.13 ‰/100 m for $\delta^{18}O$ was computed from our precipitation water samples between the Auberge and Chalet stations (with higher median value at the lower Auberge weather station), which is approximately half the isotopic lapse rates of precipitation observed in Switzerland (e.g. Beria et al., 2018). However, this lapse rate was not seen in stream water isotopes (Figure 4 a-c) measured at HyS1 (1248 masl) and HyS2 (1478 masl). The distribution of elevations feeding HyS1 (mean elevation 2165 masl) was most probably not sufficiently different from the distribution feeding HyS2 (mean elevation 2196 masl) to result in a significant shift of the isotopic values at the two streamflow sampling locations, despite the isotopic lapse rate in precipitation. The median isotopic values for the sampled springs showed an elevation gradient (Figure 4a-c, showing the spring values in order of elevation from AUBG to ICEC), except the GRAS spring, which showed a significantly higher median isotopic value. This suggests that GRAS spring might receive water only from a small low elevation sub-catchment and not from the high rock walls located next to it.
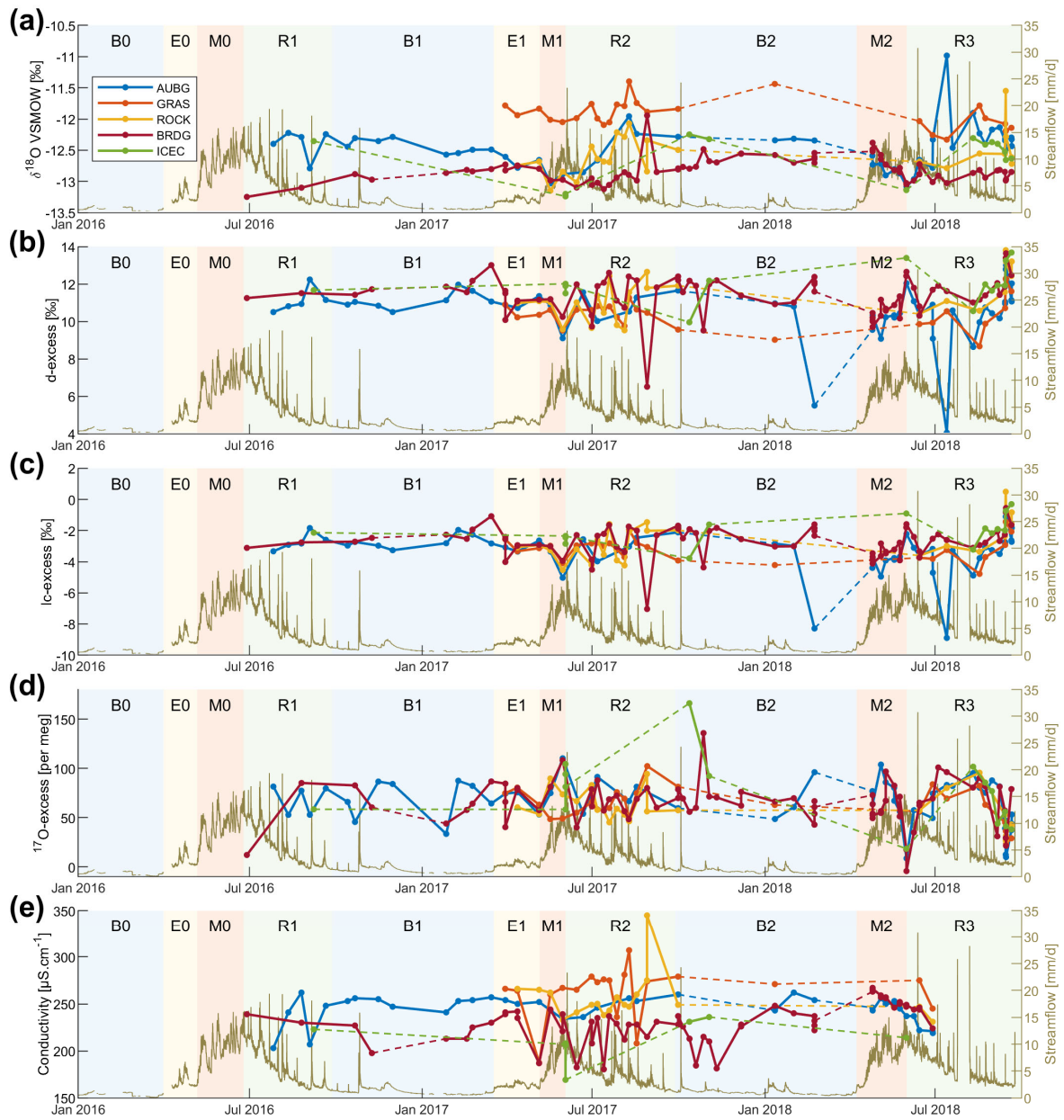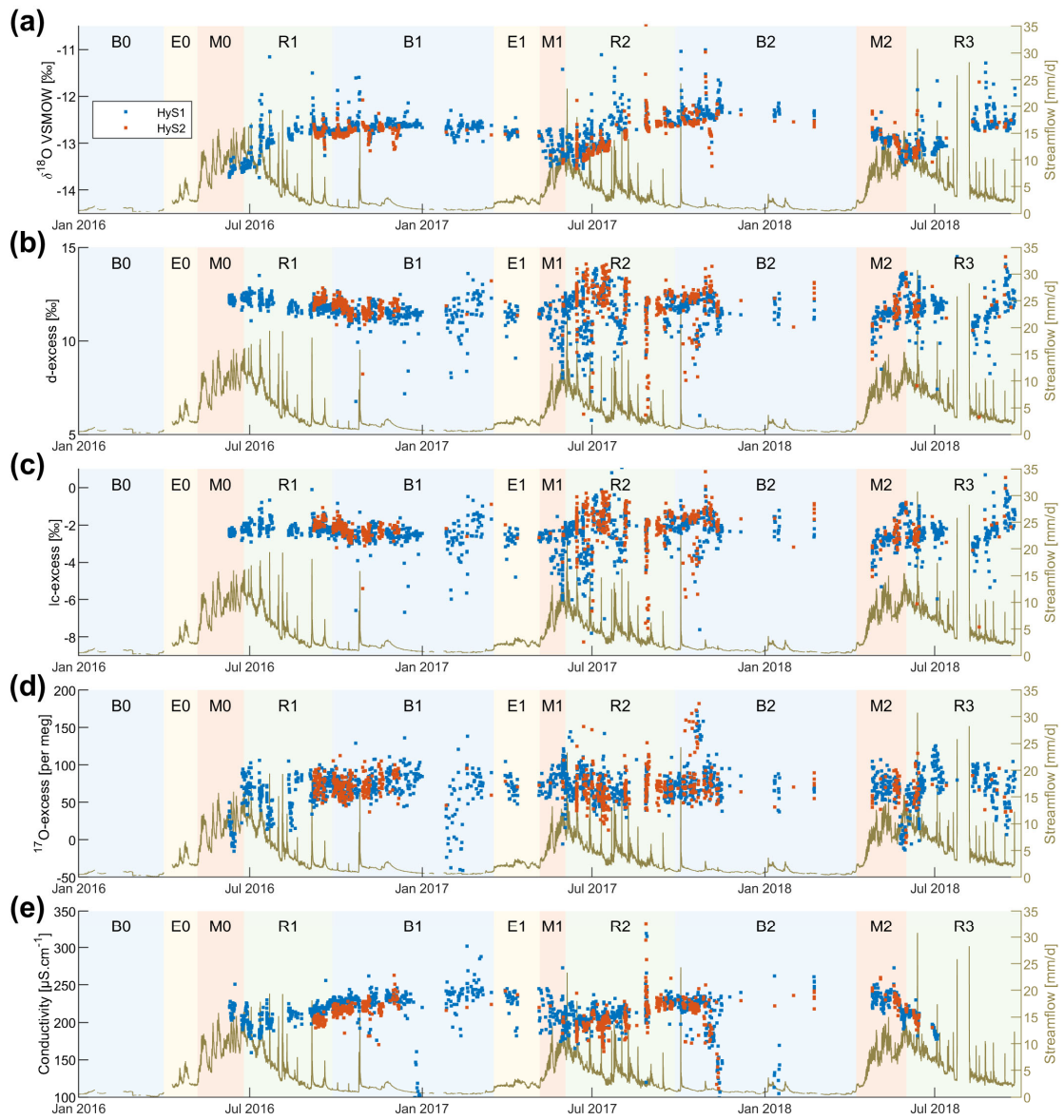
445

Figure 5. Time series of $\delta^2 H$, $\delta^{17}O$, $\delta^{18}O$, conductivity, d-excess, lc-excess and ^{17}O-excess for 5 springs (location on map Figure 1 A). We connect the dots to facilitate visualization since there are 5 separate springs traced.

Figure 6. Time series of δ²H, δ¹⁷O, δ¹⁸O, conductivity, d-excess, lc-excess and ¹⁷O-excess at the Vallon de Nant outlet HyS1 and at the upper subcatchment HyS2 (location on map Figure 1 A).
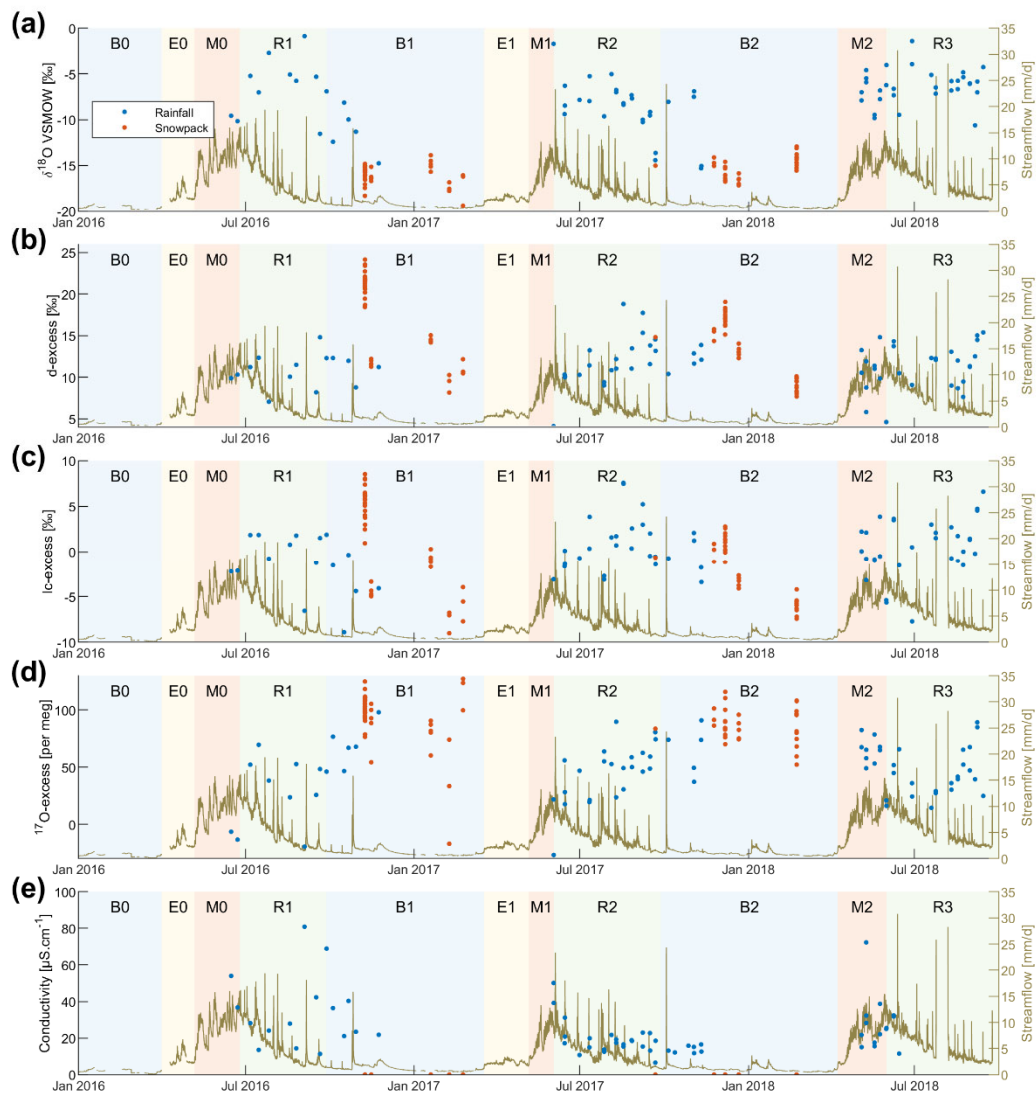
Figure 7. Time series of δ^2H, $\delta^{17}O$, $\delta^{18}O$, conductivity, d-excess, lc-excess and ^{17}O-excess for rainfall (from Auberge and Chalet weather stations, location on map Figure 1 A) and snowpack. Note that the conductivity of snowpack has not been measured.

3.5.2   Dynamics of δ^2H, $\delta^{17}O$ and $\delta^{18}O$ in springs

The fluctuations of the isotopic composition of the 6 monitored springs between July 2016 and September 2018 is discussed qualitatively based on the streamflow periods (see Figure 5). Because the variations in values of δ^2H, $\delta^{17}O$ and $\delta^{18}O$, correlate well, we will only discuss $\delta^{18}O$. Corresponding figures of the other isotopic values can be found in the supplement.

460   Despite some variability, the AUBG spring $\delta^{18}O$ values remained relatively constant ($\delta^{18}O$ between -12.8 ‰ and -12.2 ‰) during the 2016 streamflow recession R1 and then slowly decreased throughout the 2016/2017 baseflow period B1. Meanwhile, the BRDG spring started with lower isotopic values (-13.3 ‰) but got enriched in heavier isotopes through R1 and B1 to finally have a similar composition during the 2017 early melt period (E1) compared to the AUBG (and ROCK) springs, also with a subsequent decreasing trend in the heavy isotopes.

465   The 2017 minimum isotopic values of the AUBG, ROCK and BRDG springs were reached around the time of 2017 maximum streamflow and then diverged during the 2017 recession period (R2), increasing at a different rate: the δ-values of AUBG and ROCK springs increased quickly (+1.0 ‰ in 3 months), while the BRDG spring values only showed a slow increase through the winter period (B2).

        The beginning of the 2018 melt period was exceptionally fast, without an early melt period. The springs sampling started 3
470   weeks after the beginning of the early melt period (E), with a significant part of the snowpack having melted already. During M1, the isotopic composition of the AUBG and BRDG springs over this period showed a constant decrease in the heavy isotopes until the 2018 streamflow maximum. At the inverse of R1, the BRDG composition remained constant during the recession, while the AUBG spring increased quickly in the δ-values.

        The pattern repeated during the 2018 melt period (M2) with a decrease in δ-values, which then diverged at different rates.
475   Again, the BRDG spring δ-values increased slowly, while for the AUBG and ROCK springs the increase was faster.

        The ICEC spring, located on the western slopes (Figure 1), followed the same isotopic pattern as the AUBG spring. Although, because of its lower sampling rate, points were missing at the critical moments during the melting periods, which does not allow us to discuss the differences in timing. The ICEC spring showed higher isotopic values compared to BRDG even though it is located at a higher elevation, which can be explained by the higher maximum elevation of the mountain ridge upstream of
480   BRDG compared to ICEC (see Figure 1), which most certainly leads to a higher snowfall contribution to BRDG as snowmelt isotopes are more depleted in heavier isotopes than rainfall (Figure 7).

        As discussed earlier, the GRAS spring behaves differently from other springs, with higher δ-values than all the others in 2017. EC and temperature measurements indicate that this spring has relatively shallow flow paths and its δ-values also suggested a larger proportion of rainfall-derived water (which has a higher average δ-values than snowmelt; Figure 7).

485   ### 3.5.3   Dynamics of δ^2H, $\delta^{17}O$ and $\delta^{18}O$ in streamflow

        Because of the close overall correlation between $\delta^{18}O$ and δ^2H (Figure S10), and $\delta^{18}O$ and $\delta^{17}O$ values, we will highlight $\delta^{18}O$ in our discussion and figures (Figure 4-7). The temporal evolution of the isotopic values in the streamflow showed high $\delta^{18}O$ (and δ^2H) during winter baseflow, close to the median value of all sampled subsurface water bodies, and a significant decrease in the isotopic composition during the melt periods. Streamflow is thus largely fed by recent (isotopically light) snowmelt
490   during the melt period; the decrease of the $\delta^{18}O$ (or δ^2H) is proportional to the amount of snowmelt, with a larger decrease in 2017 compared to 2018. The $\delta^{18}O$ (and δ^2H) value did not decrease during E.

3.5.4   Excess (d- and lc-)

Rainfall had a median d-excess value of 11.3 ‰ and snowpack of 15.5 ‰. However, as we did not systematically sample fresh snowfall and snowpack separately, it was hard to estimate the extent of snow sublimation in Vallon de Nant.

Surface and subsurface water samples showed median d-excess values close to that of rainfall and considerably lower than the median value for snow. The apparent surface and subsurface water samples bias towards the d-excess value of rain can be explained by secondary evaporation (e.g., from soil); the soil water that remains (and that ultimately recharges groundwater and the streams) thus has a lower d-excess value than either rainfall or meltwater. Thus, the d-excess could be interpreted as the "evaporative exposure" of water during the time since precipitation, but it is rather difficult to interpret in terms of local scale process information. Even if the difference in median value between rainfall and snowfall is significant enough for a separation, because of the potential for transformation along the flow path, it will not be as valuable as the $\delta^{18}O$ (and δ^2H) values directly. For ice melt, d-excess values are too close to those of rainfall for providing further insights into its importance in streamflow.

The LMWL was calculated using linear regression between $\delta^{18}O$ and δ^2H of 75 rainfall samples with a slope of 7.38 and an intercept of 6.15 (see Figure S10). The median analytical error was 0.4 ‰ for d-excess and lc-excess, and 8 per meg for ^{17}O-excess. Compared with d-excess, LC-excess for rainfall samples indicated the spread of precipitation isotopes around the LMWL (Figure 4F). Our LMWL deviated from the GMWL. Median LC-excess of snowpack samples was close to rainfall (0 ‰), suggesting no significant snow sublimation in Vallon de Nant. The spring and stream samples showed negative median LC-excess values, indicating that recharged water has undergone some evaporation, which may vary over space and time. Out of all the springs, ICEC spring samples seemed to be less affected by evaporation (as shown by higher LC-excess value), suggesting that rainfall over the area upstream of this spring directly infiltrated into the ground. This is further supported by the presence of sparse vegetation in this part of the catchment.

3.5.5 ^{17}O-excess

We observed that snow has a median value of ^{17}O-excess of 91.3 per meg and is significantly higher than that of rainfall, 49.2 per meg. The difference between rainfall, snowpack and glacier observed for δ^2H, $\delta^{17}O$ and $\delta^{18}O$ is also visible with ^{17}O-excess, as opposed to d-excess. ^{17}O-excess could potentially be useful to distinguish between rainfall, snowpack and ice melt but secondary evaporative processes complicate a direct interpretation.

Given that the local and global reference lines for ^{17}O are very similar (see Section 2.3), it is tempting to interpret the spatial differences in ^{17}O-excess values; the median values of all sampled water show a coherent picture, with subsurface and stream water having intermediate values between rainfall and snow samples and thus being a mix thereof. As for d-excess, we can however not draw any direct conclusions on mixing ratios since rainfall and snowfall undergo further evaporative processes during recharge. Furthermore, the temporal dynamic of ^{17}O-excess in springs does not show additional information compared

to d-excess. Since use of $\delta^{17}O$ and ^{17}O-excess for tracing of alpine hydrologic processes is still relatively new, our discovery that they offer limited immediate added value is useful for future studies.

525 **4   Discussion**

4.1   Comparison with other alpine studies

Electrical conductivity of all samples are higher compared to previous such studies in Alpine environments (Cano-Paoli et al., 2019). This suggests that our site has comparatively more exchange with rocks and sediments. The temporal evolution pattern of EC that we see is typical (Penna et al., 2014; Cano-Paoli et al., 2019), as is the time lag between seasonal cycles in EC and

530 streamflow (Cano-Paoli et al., 2019). On an event-scale basis, this lag between streamflow and EC was explained by the delay between the transmission of pressure waves (leading to discharge increase) and the actual arrival of newly recharged water (Chiaudani et al., 2019).

The median $\delta^{18}O$ value of all our streamflow samples (-12.7 ‰) is slightly lower than values observed for the Rhone in Porte de Scex (Schurch et al., 2003), of which Vallon de Nant is a headwater catchment (albeit one with relatively low elevation

535 compared to other headwater catchments of the Rhone). The slightly lower values can be explained by the headwater status and thus the higher proportion of snow to rain than places lower in the basin. The isotopic lapse rate that we observe in precipitation is half that estimated for Switzerland based on data from the Global Network of Isotopes in Precipitation (GNIP) between 1966 and 2014, that is -1.9 ‰/100/m for δ^2H and -0.27 ‰/100/m for $\delta^{18}O$ (Beria et al., 2018).

Our finding that streamflow is composed of previously stored ground water rather than of recent mid-winter snowmelt from

540 hydrologically proximate areas (e.g. in the floodplain or the riparian area) based on the lack of change of $\delta^{18}O$ (and δ^2H) during E directly contradicts assumptions of some snowmelt-runoff models (Schaefli et al., 2014).

The deuterium excess (d-excess) is in the range of published values for rainfall in the Swiss Alps (Leuenberger and Ranjan, 2021) as is our higher value from snowpack (Grimsel, Schotterer et al., 2004). Higher d-excess in snowpack in these regions is related to the presence of a secondary source of winter precipitation, which comes from the Mediterranean Sea (Froehlich

545 et al., 2002) versus the dominant precipitation source being the Atlantic Ocean during majority of the year (Sodemann and Zubler, 2009). Secondary evaporative processes within the snowpack shift their isotopic ratios away from the LMWL, along the local evaporation line, causing a decrease in d-excess values (Beria et al., 2018).

Our computed ^{17}O-excess values of rainfall (Figure 4 G) are much higher than the few published values in Switzerland, which range from 6.5 per meg (Leuenberger and Ranjan, 2021) to 18 per meg (Affolter et al., 2015) for low and high elevation

550 locations. There are no published values for snowfall or snowpack for Switzerland, but values between 17 and 62 per meg for freshly precipitated snow on Mount Zugspitze (German Alps, 2962 masl) are found in the work of Surma et al. (2021). Variations in ^{17}O-excess have been found to be affected my local meteorological factors such as precipitation formation or as tracers of the evaporative conditions at the moisture source season-by-season (e.g., precipitation in summer but not in other seasons) on other continents (Midwestern North America, Tian et al., 2018). It is possible that the variations we observe are

555 limited due to the scale of our site. The difference in values between our results and those from other studies are unlikely to be related to the analytical approach used, as the normalization of the data was done using standards cross-calibrated in several laboratories also using a gas-source mass spectrometer approach. Similarly, we adopted measurement strategies to limit likely memory effects, notable for measurements of $\delta^{17}O$ values and ^{17}O-excess (Vallet-Coulomb et al., 2021). Thin snowpack has been found elsewhere to result in negative temperatures in the soil, as we measured during the 2016-2017 winter, which was

560 quite dry, at 1530 m and 2640 masl (Bender et al., 2020).

4.2 Dominant streamflow generation processes

We conceptualize the dominant hydrologic processes during different times of the year in Figure 8. During the winter baseflow period (Figure 8a), large parts of the catchment are covered with snow. Streamflow is very low as streams are mostly supplied by groundwater, with episodic melt events occurring in lower parts of the catchment. The isotopic ratios of these melt events

565 are more depleted in heavier isotopes compared to groundwater. During the early melt period (Figure 8b), the snowpack at lower elevations and close to the stream network starts releasing water to the subsurface, without melting completely. Streamflow during this period is predominantly driven by groundwater; the contributions from snowmelt and potentially rainfall at lower elevations do not lead to a change of the isotopic values of streamflow compared to the winter recession. Subsequently, snowmelt intensifies across the catchment (Figure 8c), significantly increasing the saturated subsurface areas

570 and catchment connectivity. Streamflow during this period is dominated by snowmelt (which largely flushed the subsurface water stores), resulting in very depleted isotopic ratios in stream water. Once the snowpack melts out (Figure 8d), streamflow is driven by episodic rainfall events. We will now discuss the dominant recharge processes during different parts of the year.
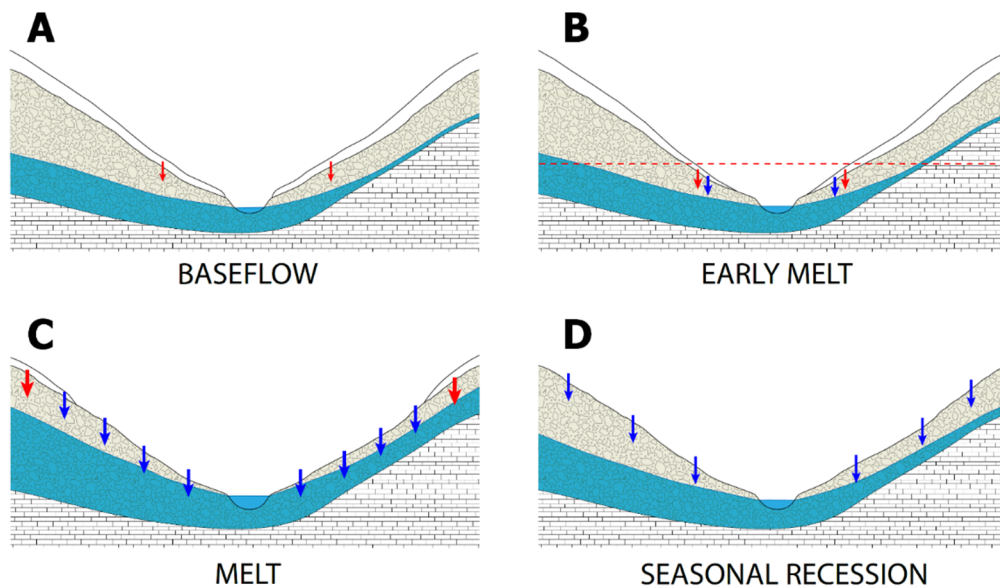
Figure 8. Conceptual figure illustrating the four streamflow generation periods: Baseflow (A), Early melt (B), Melt (C), and seasonal Recession (D). Red arrows represent water depleted in heavier isotopes (for example, snow melt), and blue arrows represents water enriched in heavier isotopes (i.e. rain). Magnitude of flux (size of arrows), location of flux, distribution of saturated area (blue), and snow cover (white) vary between the four seasons. From left to right, top to bottom: Baseflow shows a minimal contribution of snow melt to subsurface and surface even during winter; during Early melt the snow recedes at the lower elevations first (red dashed line) and contributes to streamflow; the Melt period is characterized by retreating snow cover, fluxes dominated by rain input, and small snow contributions at high elevation; Finally seasonal Recession consists only of rain inputs. Asymmetric hillslopes with differing reservoir sizes and hydraulic conductivities may produce different responses during the different phases.

4.2.1 During winter

During winter, streamflow follows a long recession curve, with almost constant baseflow between January and March. Such a constant winter baseflow can result either from a prolonged emptying of a groundwater store (Chochand et al., 2019), as assumed in many rainfall-runoff models (e.g. Mülchi et al., 2021, Staudinger et al., 2017) or from an interplay of groundwater recession and small amounts of snowmelt occurring at the snow – ground interface in absence of soil freezing (Schaefli et al., 2014). Our streamflow isotope measures suggest that streamflow is indeed resulting from a long recession and thus indicative of sufficient groundwater storage to sustain winter baseflow. However, we observed diverging trends in isotopic ratios in two springs: The lower elevation spring located near the catchment outlet (AUBG) showed depletion in heavier isotopes during winter, whereas the spring located in the higher part of the catchment (BRDG) showed enrichment in heavier isotopes (Figure 5). This suggests that there are contrasting processes at play at different elevations in Vallon de Nant during winter, which has also been reported previously in snow influenced catchments, such as in the Colorado River basin (Carroll et al., 2019). As snowmelt is more depleted in heavier isotopes compared to average annual groundwater recharge (Figure 4), the lower

elevation spring (AUBG) is likely influenced by winter snowmelt, as previously observed in other Alpine catchments (Rücker et al., 2019). However, the higher elevation spring (BRDG) is largely influenced by underlying groundwater storage, which is more enriched in the heavy isotopes compared to snowmelt (Figure 4). This is further supported by increasing trends in EC values at BRDG over the course of winters (Figure 5d), indicating the prominence of subsurface flow. The lower elevation AUBG spring shows slightly decreasing EC values over winters, confirming the presence of winter snowmelt. Thus, we conclude that in Vallon de Nant, winter baseflow at lower elevations is the combined result of a long seasonal recession and of winter snowmelt (Figure 8a). At higher elevations, winter baseflow can be largely explained by the underlying groundwater, and hence the longer seasonal recession. It is however unclear if snowmelt at lower elevations was due to atmospheric heat exchange or ground heat exchange, a question that could be interesting for future research.

4.2.2 During early spring snow melt

The early melt period is rarely discussed in the literature (for a model-based example, see the work of He et al., 2015), despite it being prevalent in Alpine regions, and the streamflow during this period remains challenging to model (see Figure 9 in Brauchli et al., 2017; or Figure 3 in Thornton et al., 2021b). In Vallon de Nant, the start of the early melt period coincides with thinning or local disappearance of the snowpack from lower elevation sites, as can be clearly seen in soil temperature measurements at lower elevations (Figure 3) (and as depicted in our sketch at Figure 8b). This suggests that streamflow rise during the early melt might be linked to snowpack melting at lower elevations. During this period, snow cover is still abundant at higher elevations as can be seen in soil temperature measurements at higher elevations (Figure 3). It is possible that snowmelt might be happening within the existing snowpack at higher elevations, but then getting retained within the snowpack (Gerdel, 1945) or be locally stored in the subsurface, and thus not leading to a strong streamflow response. An in-depth analysis is beyond the scope of this article but gives an interesting opportunity for future studies.

Interestingly, streamflow increases swiftly at beginning of E1 period, whereas EC and isotopic values (δ^2H, δ^{17}O and δ^{18}O) show a lagged response (Figure 5), suggesting that older water stored within the subsurface (with higher EC and more enriched in heavier isotopes) are first to be exfiltrated into the stream (Mcdonnell et al., 2010) at the onset of early melt. In other words, the streamflow reaction during this period is not resulting from localized snowpack outflow directly to the stream but from snowmelt transiting through the subsurface. Accordingly, during this period, streamflow rise is most likely limited by both limited snowpack outflow and temporary retention of water in the subsurface.

4.2.3 During melt periods

During the melt season, isotopic compositions of the springs converge to a common value (see M1 period in Figure 5) (around -93.5 ‰ for δ^2H, -6.8 ‰ for δ^{17}O and -13.0 ‰ for δ^{18}O), suggesting that the entire subsurface gets saturated (Figure 8c) and flushed with snowmelt. This convergence to similar values during the melt is a priori surprising because i) we have shown an isotopic lapse rate for precipitation of 0.84 ‰/(100m) for δ^2H and of 0.128 ‰/(100m) for δ^{18}O and ii) the annual median values of the isotopic values for different springs decrease with elevation (Figure 4a-c). Accordingly, the convergence of

isotopic compositions of the springs during melt to a common value strongly hints towards melt water coming from a similar
elevation range or rather towards melt water being sampled from different elevations in a similar way. This has also been seen
in previous studies in mountainous catchments (Feng et al., 2022; Penna et al., 2017).

The higher EC values in the stream at certain instances of the melt period compared to springs (Figure 5, Figure 6) are
unexpected and might suggest that there is a significant amount of subsurface water reaching the stream that has higher EC
values than all sampled springs. This result however underlines the importance of subsurface flow paths to stream recharge
during the melt periods. The positive temperature anomalies (during summer rainfall events) observed during M2 (ROCK)
show the existence of fast surface flow paths but are not enough to explain the high EC values during this period.

4.2.4   During the seasonal recession

The EC values in all springs increase during the recession period, clearly suggesting that they are all fed by subsurface water
during this period of the year. The isotopic values of the springs diverge however after the melt period, giving insights into the
underlying reservoirs that are feeding them, and their relative permeabilities and outflow rates. A smaller increase in δ-values
indicates a larger subsurface reservoir or slower flow rates/permeabilities (e.g. BRDG), where a larger increase is associated
with a smaller reservoir size or higher flow rates / permeabilities (e.g., AUBG). This difference between BRDG and AUBG
springs suggest existence of multiple subsurface reservoirs in Vallon de Nant, which has previously been observed in other
high elevation landscapes (Dwivedi et al., 2019; Mosquera et al., 2016).

The isotopic values in streamflow gradually increase over the seasonal recession period towards those of groundwater,
suggesting that groundwater becomes the dominant contributor to streamflow generation during this part of the year (Figure
6). This can also be seen in increasing EC values of streamflow in the R2 period, suggesting prevalence of deeper flow paths
over shallower flow paths. However, during large rainfall events, there are sometimes sudden increases in stream isotopic
ratio, suggesting that rainfall can become a significant contributor to streamflow generation during intense rain storms. The
role of event-based precipitation on streamflow generation has long been studied (e.g. McDonnell, 1990; Kirchner, 2003;
Kienzler and Naef, 2008) with most of the studies concluding that rainfall helps mobilize older water stored within the
catchment and that hence, the isotopic ratio in stream water often largely resembles subsurface storage (see also the metanalysis
of Barthold and Woods, 2015). Our measurements clearly suggest that this so-called "old water paradox" does not hold for
some rainfall-generated streamflow responses during the recession period. What processes might explain the fast contribution
of recent rainfall to streamwater during the recession in the Vallon de Nant remains to be studied in detail, based namely also
on our results on rainfall patterns and their relation to the stream network (Michelon et al., 2021). This analysis would however
require additional analyses of shallow groundwater dynamics and the evolution of hillslope connectivity during rainfall events.

4.3   Water temperature reveals seasonal hydrologic connectivity patterns

Temperature measurements can provide interesting insights into the seasonal evolution of hydrologic connectivity (Miralha et
al., 2023), in particular on the interaction between the alluvial plains and the hillslopes. During melt period M2, temperature

in springs BRDG and PZ3 are correlated with streamflow variations, with BRDG spring showing positive anomaly and PZ3 spring showing negative anomaly. The positive anomaly at BRDG suggests that snowmelt water traversed the landscape, got heated by direct solar radiation and then infiltrated into the spring. This argument is also supported geologically, as BRDG is recharged by snowmelt from nearby riparian areas and steep slopes facing west that are directly exposed to the sun (see Figure 1). In contrast, the negative anomaly at PZ3 suggests that snowmelt directly infiltrates during the melt period, also seen in the nearby areas that become snow free quickly (200m distance from soil temperature sensor at 1530 masl). This clearly differentiates the local snowmelt processes (in the order of tens of meters) from the more regional snowmelt patterns (in the order of few hundred meters).

Additionally, temperature measurement provides insight into groundwater connectivity. Water temperatures are usually influenced by ground temperature, but the high hydraulic conductivity in areas surrounding PZ3 does not allow enough time for the water temperature to reach equilibrium. This temporary (6 weeks) and local snowmelt input is superimposed on a longer scale pattern that leads to 74 days of lag between PZ3 and air temperature. This suggests that subsurface in Vallon de Nant gets fully saturated and well-connected during melt periods, and less connected during later part of the year (also depicted in Figure 8c). This was also highlighted by stable water isotope measurements discussed in preceding sections, where the entire catchment becomes well connected during melt periods (Figures 5, 6).

The lags in water temperature can indicate the reactivity of the subsurface flow. The PZ1 spring (470 m to the north) reacts in a different way, with a 58-day lag indicating a shallower flow path, but without temperature anomaly during the melt period. Short-term temperature anomalies (positive during the summer, negative during the winter) associated with rainfall events suggest local incursions of surface water, which is in contradiction with the absence of temperature anomalies during the melting period. One possible explanation is that the subsurface volume feeding this spring is small enough (with water levels between 0.8 and 2.4 m below the surface, see Supplementary Material, Figure S8) during R2 and B2 to react quickly to local surface inputs, while during M2 period volume increases significantly (with water level between 0.1 and 1.0 m below the surface) to not show short term reactions to melt water input. This highlights a very dynamic subsurface system.

Average temperature of subsurface water provides insight regarding the origin of the water. The average temperature difference between PZ1 and PZ3 (mean 6.3°C and 4.8°C over the year) can most likely be explained by their respective sub catchments: PZ1 (left bank) collects water from the grassy slopes of the west side of the valley (facing east), while through PZ3 (right bank) flows water from the south (facing north), with more shaded areas and snowpack remaining later in the year.

At the end of B2, temperature at the 4 springs converge to 4.3°C and if we limit ourselves only to this variable, we could think that this is pointing toward a common aquifer feeding them during baseflow. The shift of the PZ1 and PZ3 temperatures (+0.4 °C and -0.5 °C) at the end of baseflow could be explained by an unconfirmed contamination issue, specifically of air into the piezometers. The fact that isotope composition of the water in the streamflow during B2 is close to the median value of all sampled water sources suggests that our spatial sampling was good enough to represent the main water sources during baseflow.

The EC measurements clearly suggest that the subsurface flow path distributions are very similar in the upper part of the catchment (HyS2) and in the lower part of the catchment (HyS1). This is further supported by the fact that the isotopic lapse rate measured in rain water does not translate into streamflow.

The isotopic composition of GRAS is quite different from the other sources (mean values of -85.3 ‰ for δ^2H, -6.3 ‰ for $\delta^{17}O$ and -12.0 ‰ for $\delta^{18}O$). The absence of a temperature anomaly during the melt period suggests a large and well-mixed source of water. The high thermal connectivity with the surface could then be explained by a shallow flow path over a certain distance before the water exits at the source. However, we still cannot explain why the temperature signal shows a variation induced by rainfall, whereas there is no variation due to snowmelt input.

4.4 Transferable insights

4.4.1 Temperature of water origin and shallow soil

Although temperature is not a conservative tracer, temperature measurements of springs are useful to estimate flow path depth. We provide a quantitative tool in the Appendix 2. However, the underlying assumption of our method that heat transfer is driven by conduction might not always be verified (Kane et al., 2001), and anomalies between measured and modelled temperature (pure sinusoid) could be related to heat transport with subsurface water flows (i.e. to advection phenomena).

At shallow depths (10 cm), soil temperature is strongly influenced by air temperature, and our analysis of soil temperature at different elevations shows that it can be used as a good proxy for detection of snow cover. Early melt starts when the soil temperature at low elevation (1240 masl) rises, showing that snow is melting near the catchment outlet. The soil temperature sensor, albeit not intended for this use, seems to be well positioned to detect the onset of early melt at lower elevations.

For the other soil temperature recordings at higher elevations, there is no direct link to streamflow dynamics. The time elapsed between snowcover disappearance at the soil temperature site at 1530 masl and the beginning of the melting period varies significantly but is always positive (8 days in 2016, 3 days in 2017 and 51 days in 2018), underlying that intermediate elevations are actively contributing snowmelt water during the rise of the melt period. For the highest site, there can be some snow left at the beginning of the recession period.

Other studies have also observed the reactivity of soil temperature to snowpack depth. Bender et al. (2020) observed that in general ground temperature is more stable under thicker snowpacks and that high level of temperature variability in ground temperature mainly occurs when the snowpack is absent, but they do notice that under thin snowpacks, ground temperature can fluctuate dramatically, though without heating, perhaps suggesting the presence of sub-snowpack moisture flow. In fact, they showed that vegetation combined with thin snow delayed the ground warming.

A larger number of soil temperature sensors would provide an interesting perspective to identify more precisely the relative contributions of the different landscape units, elevations, and terrain aspects. This could be particularly promising in combination with satellite images for snow cover mapping.

4.4.2 Isotopic composition of springs and stream water

Stable isotopes of water are particularly promising to track the co-existence of seasonal baseflow and winter melt within springs and shallow groundwater. However, this requires a year-round time series to observe where and when isotopic ratios in groundwater becomes enriched or depleted. This year-round monitoring is particularly important as many subsurface signals are likely to see a "reset" during the main melt period, as highlighted in our work here.

The range of isotopic composition for each water source informs on the relative snowmelt proportions from their respective sub-catchments. Without evidence of a strong isotopic lapse rate in snowfall, the differences measured can be explained by the variation of snowfall amounts with elevation.

The relative proximity of some water sources monitored in this study underlines that spatial proximity does not necessary imply similar behaviors (in terms of temperature or isotopic composition), as we see noticeable differences between the sources due to the different characteristics of their sub catchments (i.e. flow path depth, hydraulic conductivity, slope, aspect).

LC-excess values might reveal some additional insights in future work, in combination with future analyses of soil water isotopes (to give insights into evaporation effects).

At this stage, it is not clear either what the value of ^{17}O-excess is for hydrological purposes and the question whether it conveys local scale information remains open. These measures would have probably been more relevant if fresh snow was sampled instead of the snowpack. Even if we cannot draw any interesting conclusions, the publication of these values will nevertheless be useful for future work.

4.4.3 The added value of EC

EC allows qualitative estimation of stream water sources and is very useful to distinguish periods where streamflow is dominated by snowmelt vs groundwater. During periods of high snowmelt, a drop in stream EC can be explained by dilution from meltwater (Chiaudani et al., 2019), which has shorter subsurface residence time vs older water stored within the subsurface, and accordingly a lower ionic content and EC (Cano-Paoli et al., 2019). However, the difficulty to characterize the different physical and geochemical properties of soils (influencing EC) do not allow an intercomparison of absolute EC values between the sources. However, variations at a given source may inform on the snowmelt input (low EC) or the flow path dynamic (old water pushed by water input). In catchments like Vallon de Nant that exhibit little elevational gradients in stream isotopic ratios, EC represents an extremely valuable tracer to segregate the relevance of snowmelt in streamwater generation.

4.4.4 The uncertain value of δ^{17}O and ^{17}O-excess

The d-excess and ^{17}O-excess are typically used to investigate the large-scale hydrological cycle and oceanic moisture sources (Nyamgerel et al., 2021). Both d-excess and ^{17}O-excess respond to relative humidity during evaporative processes but ^{17}O-excess may be less temperature sensitive (Surma et al., 2021; Bershaw et al., 2020) than d-excess and thus indicate compositions of evaporation and climatic conditions even when they would be invisible with d-excess (Risi et al., 2010). Much

laboratory time was devoted here to the measurement of $\delta^{17}O$ and ^{17}O-excess, without providing conclusive insights or specific added value for documenting the influence of local-scale snow dynamics, specifically the variation in space and time of accumulation, transport, storage, melt and sublimation, on hydrological processes, except some unvalidated potential to distinguish glacier melt from snowmelt when combined with temperature measurements. This is partly also due to absence of relevant reference data. We hope that the full value of the $\delta^{17}O$ data set presented here will be investigated and disentangled in the future.

5   Conclusion

This paper focuses on understanding the interplay of runoff generation processes in all four seasons in the high Alpine Vallon de Nant catchment using four tracers: water and soil temperature, EC, stable water isotopes. Furthermore, we discuss the value of these four tracers for hydrologic process investigation for comparable catchments.

Streamflow generation in Vallon de Nant is the outcome of a complex temporal succession of surface and subsurface contributions that can be best understood by starting the analysis at the observed "reset" of the isotopic composition during the melt period. During this reset, isotopic composition of the springs converge, the entire subsurface gets saturated and flushed with snowmelt that either comes from a similar elevation range or gets sampled from different elevations. Accordingly, interpretation of the isotopic dynamics becomes extremely complicated and the value of year-round water isotope samples might be reduced to being a simple measure of the relative proportions of snowmelt compared to rainfall in the different sampled water sources.

The sampled EC values, in addition to isotopes, give further insights into subsurface exchanges in the Vallon de Nant catchment. Together, the isotopic composition and the EC values suggest that i) subsurface flow plays a prominent role through all stages of snowmelt and that ii) winter streamflow might be composed of both local winter snowmelt and groundwater contributions that are recharged on an annual basis. Temperature measurements in springs and soil across elevation gradients provide additional insights into flow path depth and highlights the effect of rain-on-snow events on soil temperature below the snowpack, though they are undetectable in discharge.

Based on our case-study specific conclusions, our take home messages for future work at other locations are:

- Understanding the dynamics of stable water isotopes in comparable high-elevation catchments requires sampling their potential reset during the snow melt period, which necessitates collecting samples year-round or at a minimum, starting very early in the melt season (which is often impossible responsibly at avalanche-prone locations).

- Such a reset makes the interpretation of stable water isotopes samples from different surface and subsurface water sources particularly challenging and a combination with other tracers might be required for all similar studies. We recommend that EC monitoring be explored as a more direct indicator of water age and subsurface flow. Water temperature is recommended to add insights into how well different water stores are connected. Combined with EC,

water temperature has a particular added value to disentangle shallow from deeper flow paths (as both can have high EC).

- Appropriate characterization of the variability of all tracers studied here (water and soil temperature, EC, stable water isotopes) requires sampling during the winter baseflow period, which is, again, a challenge at many places.

- Characterisation of different streamflow generation periods and processes can greatly benefit from continuous soil temperature measurements, which give information on presence and absence of an insulating snowpack and on potential disconnection of the subsurface in case of soil freezing. We recommend systematic soil temperature measurements in comparable hydrological process studies.

- Winter melt and runoff generation processes might be more present at high elevations than previously thought. These winter processes potentially condition the catchment-scale hydrologic response during the melt period and groundwater recharge at the annual scale. Future work on this topic should also revisit the concepts that correspond to this field-scale process in hydrologic models.

Appendix 1: Influence of air on the isotopic composition of a water sample (δ^2H, $\delta^{17}O$ and $\delta^{18}O$) within a sealed container

820 The purpose of this calculation is to estimate how the isotopic composition of a water sample locked up together with some air in a sealed container will be altered by the water vapor of the air. This configuration may happen i.e. with snow sampling as snow density ranging from 0.55 to 0.83 suggests that at least 17 % to 45 % of the volume in the container is ambient air from the sampling site. To make these calculations we consider the conditions in which the samples will be analysed; we take the ambient temperature of 25.3 °C for which we know the isotopic fraction factor between vapor and liquid phases of water

825 for δ^2H, $\delta^{17}O$ and $\delta^{18}O$. At this temperature the samples are in a liquid phase, and in equilibrium with the air of their container. Following Mook et al. (2008), the isotopic fractionation of water between two phases at the equilibrium is written as a reaction between the liquid l and vapor v phases of H_2O as:

$$H_2O_l + H_2O^*{}_v \leftrightarrow H_2O^*{}_l + H_2O_g, \qquad\qquad (1)$$

where * marks the heavy isotopic form of the molecule that may contain ^2H, ^{17}O or ^{18}O, and δ^* its isotopic composition in

830 per mil. At a given temperature T, the isotopic fractionation factor of water between liquid and vapor $\propto_{l/v}$ is the equilibrium constant of the Equation 1:

$$\propto_{l/v}(T) = \frac{[H_2O^*]_l[H_2O]_v}{[H_2O]_l[H_2O^*]_v} = \frac{\delta^*_l/1000+1}{\delta^*_v/1000+1} \qquad\qquad (2)$$

As we know i) the amount of liquid water in the container and its initial isotopic composition, ii) the amount of ambient air captured in the container and its initial isotopic composition, and that we can deduce iii) the total amount of heavy isotopes in

835 the total amount of water, we can solve the Equation 2 as a second order equation.

The calculations are made for two extreme amounts of air vapor saturation, namely air without any water vapor and air fully saturated with water vapor. For the last one we take the partial pressure of water at 25°C P=3169.9 Pa (Haynes et al., 2017):

The value of the fractionation factor of water ^2H and ^{18}O between 0 and 100°C are (Majoube, 1971):

$$ln\ ^2\!\propto_{l/v}(T) = 24.844.10^3/T^2 - 76.248/T - 52.612.10^{-3} \qquad\qquad (3)$$

840 $$ln\ ^{18}\!\propto_{l/v}(T) = 1.137.10^3/T^2 - 0.4156/T - 2.0667.10^{-3} \qquad\qquad (4)$$

From Equations 3 and 4 we compute $^2\!\propto_{l/v}(T = 25.3\ °C) = 1.0789$ and $^{18}\!\propto_{l/v}(T = 25.3\ °C) = 1.0135$.

For ^{17}O we will take the experimental values given by Barkan and Luz (2005) at 25.3 °C: $^{17}\!\propto_{l/v} = 1.00496 \pm 0.00002$.

For each stable water isotope, the values are calculated for 2 extreme sample isotopic composition from our database (δ^2H = -180 ‰ and 5 ‰, $\delta^{17}O$ = -12 ‰ and 0 ‰, $\delta^{18}O$ = -30 ‰ and 5 ‰). The range of the isotopic composition of ambient air is

845 based on records reported by Wei et al. (2019) for Rietholzbach, Switzerland (755 masl) from August to December 2011: the δ^2H air values range between -239.79 ‰ and -73.48 ‰, and $\delta^{18}O$ values range between -31.41 ‰ and -9.94 ‰. No reference value is available for $\delta^{17}O$, so a range between -30 and 0 ‰ has been chosen arbitrarily.

The Figure shows the changes of the sample isotopic composition for δ^2H, $\delta^{17}O$ and $\delta^{18}O$. These values have been completed for different amounts of air (ratios of sample volume over container volume).

850   The constant error for dry air corresponds to the case where the water vapor in air originates via evaporation of the water sample.
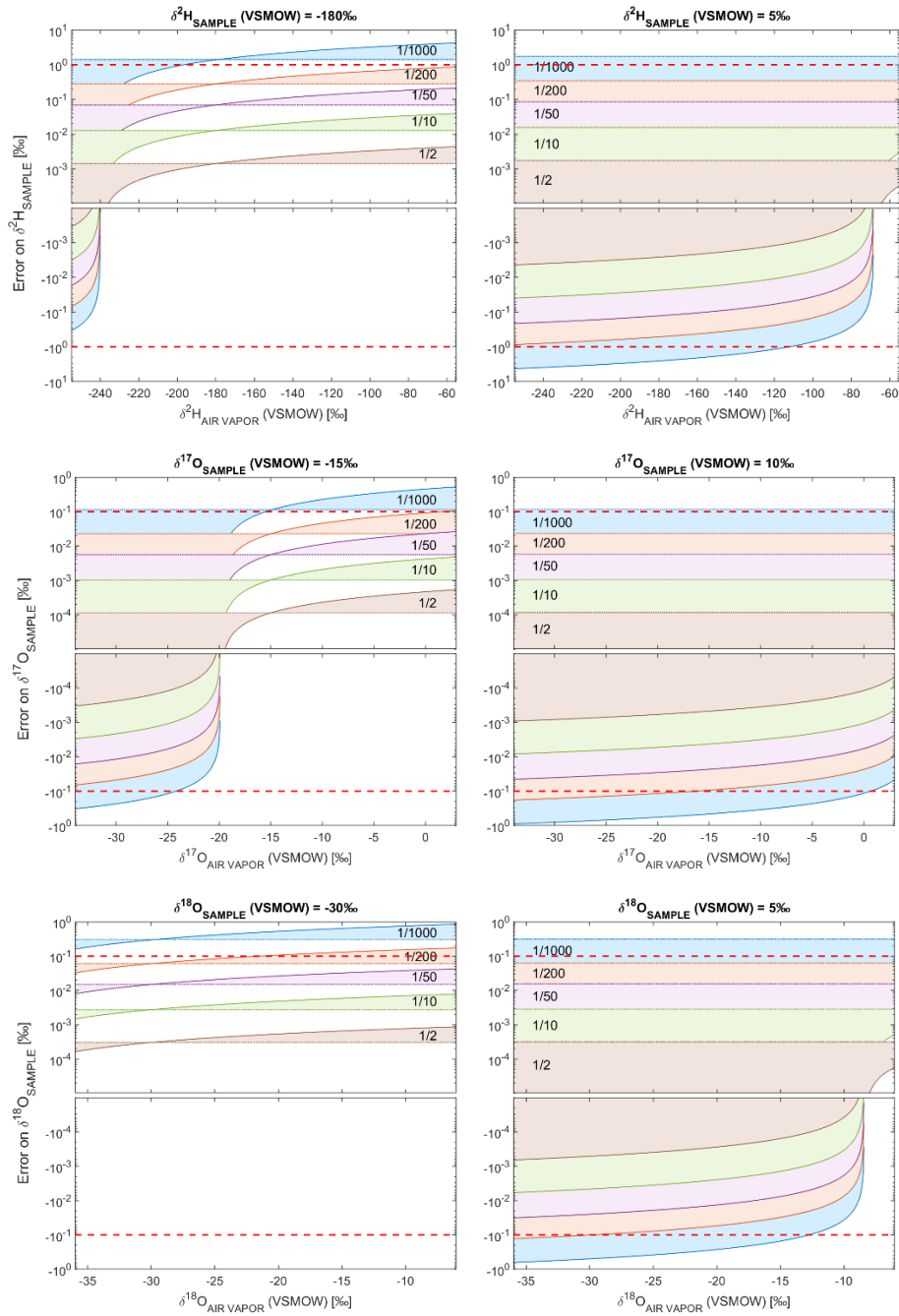
855   Figure A1: Changes in δ^2H, $\delta^{17}O$ and $\delta^{18}O$ of a water sample depending on the initial isotopic composition of the water vapor of the air locked up with the sample. The results are completed for saturated air (continuous line) and dry air (dashed line), for ratios of sample volume over container volume from 1/2 to 1/1000. The red dashed line represents the detection limit of the measuring device.

Appendix 2: Estimate of water flow depth based on a soil temperature model

The estimate of the water flow depth is based on the soil temperature model presented in the work of Elias et al. (2004), assuming the water temperature measured at the spring/piezometer being equal to the soil temperature at the mean water flow depth. The evolution with time t of soil temperature T at the surface (depth $z=0$) corresponds to air temperature, and is characterized by the mean air temperature T_a and its amplitude A:

$$T(z=0, t) = T_a + A \sin(\omega t + \varphi), \tag{4}$$

with ω the radial frequency (in rad/s) and φ a phase constant (in rad). The heat transfer into the soil is dampened by D, the dampening depth coefficient (in m) expressed as a function of K (in m²/s) the soil thermal diffusivity:

$$D = \sqrt{\frac{2K}{\omega}}, \tag{5}$$

giving the soil temperature at depth z:

$$T(z, t) = T_a + A \exp\left(-\frac{z}{D}\right) \sin\left(\omega t - \left(\frac{z}{D}\right) + \varphi\right), \tag{6}$$

The lag time L between air temperature and soil temperature at a given depth z is then:

$$L(z) = \frac{z}{\omega D}. \tag{7}$$

The depth is approached using the *fminsearch* function in MatLab, reducing the error between the observed lag time and the modelized lag time. Although the thermal diffusivity of soil is influenced by i) water volumetric content, ii) volume fraction of solids, and iii) air-filled porosity (Ochsner et al., 2001), we retain for this computation a unique value of thermal diffusivity of soil for all the points, using the typical value of $5.56.10^{-7}$ m²/s (Elias et al., 2004). The sinusoidal air temperature is based on time series from a grided product (1 x 1 km grid) from MeteoSuisse (Schaefli, 2021). The results are presented in Table 2 and Figure A2.

Table 2. Characteristics of the sinusoidal air and water temperatures used for the soil temperature model, and characteristics of the soil temperature at the estimate depth corresponding to the water temperature.

Water sources	Measured air T [°C]		Measured water T [°C]		Air/Water lag time [d]	Modelized soil T [°C]		Modelized Soil depth [m]
	mean	*amplitude*	*mean*	*amplitude*		*mean*	*amplitude*	
PZ1	5.8	10	6.3	3.8	79	6	5.1	3.2
PZ3	5.8	10	4.8	3.7	105	4.5	3.3	4.3
GRAS	6.3	10	5.5	3	41	5.3	9.9	1.7
ROCK	6.3	10	5.4	2.5	39	5.2	10.2	1.6
BRDG	5.8	10	4.7	0.9	6	5	18	0.2
ICEC	5.8	10	4.3	0.4	133	4.2	2	5.4
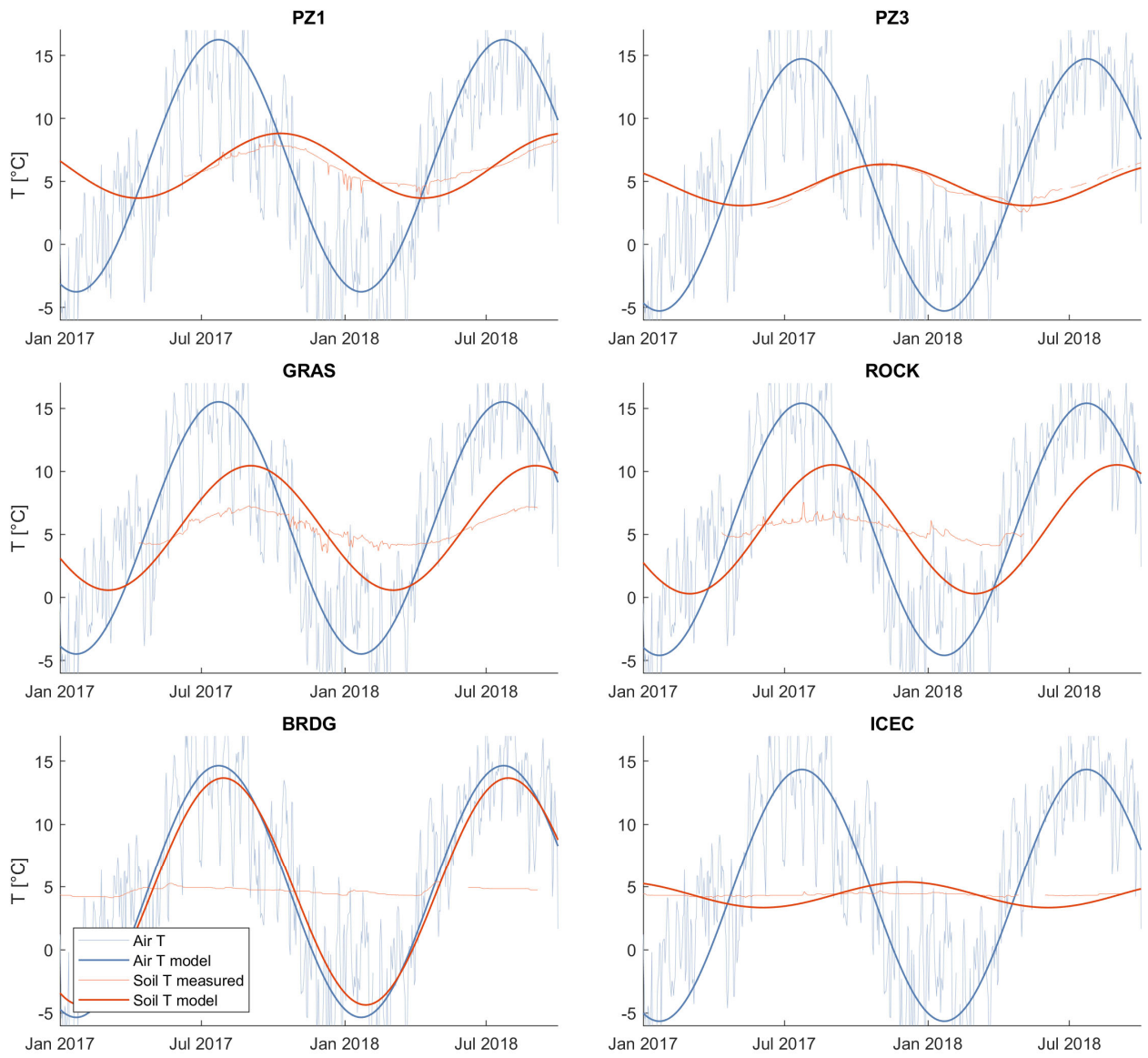
885   Figure A2: Measured and modelized air and soil temperature for 2 piezometers (PZ1 and PZ3) and 4 springs (GRAS, ROCK, BRDG and ICEC).

References

Affolter, S., Hauselmann, A. D., Fleitmann, D., Hauselmann, P., and Leuenberger, M.: Triple isotope (delta D, delta O-17, delta O-18) study on precipitation, drip water and speleothem fluid inclusions for a Western Central European cave (NW Switzerland), Quaternary Sciences Review, 127, 73-89, 10.1016/j.quascirev.2015.08.030, 2015.

Antoniazza, G., Nicollier, T., Boss, S., Mettra, F., Badoux, A., Schaefli, B., Rickenmann, D., and Lane, S.: Hydrological drivers of bedload transport in an Alpine watershed, Water Resources Research, 58, e2021WR030663, 10.1029/2021WR030663, 2022.

Arnoux, M., Brunner, P., Schaefli, B., Mott, R., Cochand, F., and Hunkeler, D.: Low-flow behavior of alpine catchments with varying quaternary cover under current and future climatic conditions, J. Hydrol., 125591, 10.1016/j.jhydrol.2020.125591, 2020.

Badoux, H.: Aperçu géologique du Vallon de Nant. La Thomasia, Jardin alpin de Pont de Nant., Lausanne, 37-43, 1991.

Barkan, E. and Luz, B.: High precision measurements of O-17/O-16 and O-18/O-16 ratios in H2O, Rapid Rapid Commun Mass Sp, 19, 3737-3742, 10.1002/rcm.2250, 2005.

Barthold, F. K., and Woods, R. A.: Stormflow generation: A meta-analysis of field evidence from small, forested catchments, Water Resources Research, 51, 3730-3753, 10.1002/2014WR016221, 2015.

Bender, E., Lehning, M., and Fiddes, J.: Changes in Climatology, Snow Cover, and Ground Temperatures at High Alpine Locations, Frontiers in Earth Science, 8, 10.3389/feart.2020.00100, 2020.

Benoit, L., Allard, D., and Mariethoz, G.: Stochastic Rainfall Modeling at Sub-kilometer Scale, Water Resources Research, 54, 4108-4130, 10.1029/2018WR022817, 2018.

Beria, H., Larsen, J. R., Michelon, A., Ceperley, N. C., and Schaefli, B.: HydroMix v1.0: a new Bayesian mixing framework for attributing uncertain hydrological sources, Geosci. Model Dev., 13, 2433-2450, 10.5194/gmd-13-2433-2020, 2020.

Beria, H., Larsen, J. R., Ceperley, N. C., Michelon, A., Vennemann, T., and Schaefli, B.: Understanding snow hydrological processes through the lens of stable water isotopes, Wires Water, 5, 10.1002/wat2.1311, 2018.

Beria, H.: Improving hydrologic model realism using stable water isotopes in the Swiss Alps, PhD thesis, Institute of Earth Surface Dynamics, Faculty of Geosciences and the Environment, University of Lausanne, Lausanne, https://serval.unil.ch/resource/serval:BIB_F160C96E9030.P002/REF, 2020.

Bershaw, J., Hansen, D. D., and Schauer, A. J.: Deuterium excess and O-17-excess variability in meteoric water across the Pacific Northwest, USA, Tellus B, 72, 10.1080/16000889.2020.1773722, 2020.

Blahusiakova, A., Matouskova, M., Jenicek, M., Ledvinka, O., Kliment, Z., Podolinska, J., and Snopkova, Z.: Snow and climate trends and their impact on seasonal runoff and hydrological drought types in selected mountain catchments in Central Europe, Hydrol. Sci. J.-J. Sci. Hydrol., 65, 2083-2096, 10.1080/02626667.2020.1784900, 2020.

Brauchli, T., Trujillo, E., Huwald, H., and Lehning, M.: Influence of Slope-Scale Snowmelt on Catchment Response Simulated With the Alpine3D Model, Water Resources Research, 53, 10723-10739, 10.1002/2017wr021278, 2017.

Brighenti, S., Tolotti, M., Bruno, M. C., Engel, M., Wharton, G., Cerasino, L., Mair, V., and Bertoldi, W.: After the peak water: the increasing influence of rock glaciers on alpine river systems, Hydrological Processes, 33, 2804-2823, 10.1002/hyp.13533, 2019.

Brunner, M. I., Farinotti, D., Zekollari, H., Huss, M., and Zappa, M.: Future shifts in extreme flow regimes in Alpine regions, Hydrol. Earth Syst. Sci., 23, 4471-4489, 10.5194/hess-23-4471-2019, 2019.

Cano-Paoli, K., Chiogna, G., and Bellin, A.: Convenient use of electrical conductivity measurements to investigate hydrological processes in Alpine headwaters, Sci. Total Environ., 685, 37-49, 10.1016/j.scitotenv.2019.05.166, 2019.

930 Carroll, R. W. H., Deems, J. S., Niswonger, R., Schumer, R., and Williams, K. H.: The Importance of Interflow to Groundwater Recharge in a Snowmelt-Dominated Headwater Basin, Geophys Res Lett, 46, 5899-5908, 10.1029/2019GL082447, 2019.

Ceperley, N., Zuecco, G., Beria, H., Carturan, L., Michelon, A., Penna, D., Larsen, J., and Schaefli, B.: Seasonal snow cover decreases young water fractions in high Alpine catchments, Hydrological Processes, 34, 4794-4813, 10.1002/hyp.13937, 2020.

935 Ceperley, N., Michelon, A., Escoffier, N., Mayoraz, G., Boix Canadell, M., Horgby, A., Hammer, F., Antoniazza, G., Schaefli, B., Lane, S., Rickenmann, D., and Boss, S.: Salt gauging and stage-discharge curve, Avançon de Nant, outlet Vallon de Nant catchment, Zenodo, 10.5281/zenodo.1154798, 2018.

Cherix, D. and Vittoz, P.: Synthèse et conclusions aux Journées de la biodiversité 2008 dans le Vallon de Nant, Biodiversité du Vallon de Nant, Mémoire de la Société vaudoise des Sciences naturelles, 23, 225-240, 2009.

940 Chiaudani, A., Di Curzio, D., and Rusi, S.: The snow and rainfall impact on the Verde spring behavior: A statistical approach on hydrodynamic and hydrochemical daily time-series, Sci. Total Environ., 689, 481-493, 10.1016/j.scitotenv.2019.06.433, 2019.

Cochand, M., Christe, P., Ornstein, P., and Hunkeler, D.: Groundwater Storage in High Alpine Catchments and Its Contribution to Streamflow, Water Resources Research, 55, 2613-2630, 10.1029/2018wr022989, 2019.

945 Constantz, J.: Heat as a tracer to determine streambed water exchanges, Water Resources Research, 44, 10.1029/2008WR006996, 2008.

Coplen, T. B.: Reporting of Stable Hydrogen, Carbon, and Oxygen Isotopic Abundances, Pure Appl Chem, 66, 273-276, 10.1351/pac199466020273, 1994.

Dansgaard, W.: Stable Isotopes in Precipitation, Tellus, 16, 436-468, 1964.

950 Dutoit, A.: La Végétation de l'étage Subalpin Du Vallon de Nant, PhD thesis, University of Lausanne, Switzerland, 131, 1983.

Dwivedi, R., Meixner, T., McIntosh, J. C., Ferré, P. A. T., Eastoe, C. J., Niu, G. Y., Minor, R. L., Barron-Gafford, G. A., and Chorover, J.: Hydrologic functioning of the deep critical zone and contributions to streamflow in a high-elevation catchment: Testing of multiple conceptual models, Hydrological Processes, 33, 476-494, 10.1002/hyp.13363, 2019.

955 Elias, E. A., Cichota, R., Torriani, H. H., and de Jong van Lier, Q.: Analytical soil-temperature model: correction for temporal variation of daily amplitude, Soil Science Society of America Journal, 68, 784-788, 10.2136/sssaj2004.7840, 2004.

Engel, M., Penna, D., Bertoldi, G., Dell'Agnese, A., Soulsby, C., and Comiti, F.: Identifying run-off contributions during melt-induced run-off events in a glacierized alpine catchment, Hydrological Processes, 30, 343-364, 10.1002/hyp.10577, 960 2016.

Feng, M., Zhang, W., Zhang, S., Sun, Z., Li, Y., Huang, Y., Wang, W., Qi, P., Zou, Y., and Jiang, M.: The role of snowmelt discharge to runoff of an alpine watershed: Evidence from water stable isotopes, J. Hydrol., 604, 127209, 10.1016/j.jhydrol.2021.127209, 2022.Floriancic, M. G., van Meerveld, I., Smoorenburg, M., Margreth, M., Naef, F., Kirchner, J. W., and Molnar, P.: Spatio-temporal variability in contributions to low flows in the high Alpine Poschiavino 965 catchment, Hydrological Processes, 32, 3938-3953, 10.1002/hyp.13302, 2018.

Foster, L. M., Bearup, L. A., Molotch, N. P., Brooks, P. D., and Maxwell, R. M.: Energy budget increases reduce mean streamflow more than snow-rain transitions: using integrated modeling to isolate climate change impacts on Rocky Mountain hydrology, Environ. Res. Lett., 11, 10, 10.1088/1748-9326/11/4/044015, 2016.

Freudiger, D., Frielingsdorf, B., Stahl, K., Steinbrich, A., Weiler, M., Griessinger, N., and Seibert, J.: The Potential of meteorological gridded datasets for hydrological modeling in alpine basins, Hydrol Wasserbewirts, 60, 353-367, 10.5675/HyWa_2016,6_1, 2016.

Froehlich, K., Gibson, J. J., and Aggarwal, P. K.: Deuterium excess in precipitation and its climatological significance, International Atomic Energy Agency (IAEA) 2002.

Gallice, A., Schaefli, B., Lehning, M., Parlange, M. B., and Huwald, H.: Stream temperature prediction in ungauged basins: review of recent approaches and description of a new physics-derived statistical model, Hydrology and Earth System Sciences, 19, 3727-3753, 10.5194/hess-19-3727-2015, 2015.

Gerdel, R. W.: The dynamics of liquid water in deep snow-packs, Trans. AGU, 26, 83, 10.1029/TR026i001p00083, 1945.

Giaccone, E., Luoto, M., Vittoz, P., Guisan, A., Mariéthoz, G., and Lambiel, C.: Influence of microclimate and geomorphological factors on alpine vegetation in the Western Swiss Alps, Earth Surface Processes and Landforms, 44, 3093– 3107, 10.1002/esp.4715, 2019.

Grand, S., Rubin, A., Verrecchia, E. P., and Vittoz, P.: Variation in Soil Respiration across Soil and Vegetation Types in an Alpine Valley, Plos One, 11, 10.1371/journal.pone.0163968, 2016.

Hammond, J. C. and Kampf, S. K.: Subannual Streamflow Responses to Rainfall and Snowmelt Inputs in Snow-Dominated Watersheds of the Western United States, Water Resources Research, 56, 10.1029/2019WR026132, 2020.

Hanus, S., Hrachowitz, M., Zekollari, H., Schoups, G., Vizcaino, M., and Kaitna, R.: Future changes in annual, seasonal and monthly runoff signatures in contrasting Alpine catchments in Austria, Hydrology and Earth System Sciences, 25, 3429-3453, 10.5194/hess-25-3429-2021, 2021.

Hayashi, M.: Alpine Hydrogeology: The Critical Role of Groundwater in Sourcing the Headwaters of the World, Groundwater, 58, 498-510, 10.1111/gwat.12965, 2020.

Haynes, W. M., Lide, D. R., and Bruno, T. J.: CRC handbook of chemistry and physics, Boca Raton, Florida : CRC Press/Taylor & Francis, 10.1201/b17118, 2017.

He, Z. H., Tian, F. Q., Gupta, H. V., Hu, H. C., and Hu, H. P.: Diagnostic calibration of a hydrological model in a mountain area by hydrograph partitioning, Hydrology and Earth System Sciences, 19, 1807-1826, 10.5194/hess-19-1807-2015, 2015.

Horgby, A., Canadell, M. B., Utseth, A. J., Vennemann, T. W., and Battin, T. J.: High-Resolution Spatial Sampling Identifies Groundwater as Driver of CO2 Dynamics in an Alpine Stream Network, J Geophys Res-Biogeo, 124, 1961-1976, 10.1029/2019jg005047, 2019.

Huggenberger, P.: Faltenmodelle und Verformungsverteilung in Deckenstrukturen am Beispiel der Morcles-Decke (Helvetikum der Westschweiz), Ph.D. Thesis, ETH-Zürich, Switzerland, 326, 10.3929/ethz-a-000365939, 1985.

Kane, D. L., Hinkel, K. M., Goering, D. J., Hinzman, L. D., and Outcalt, S. I.: Non-conductive heat transfer associated with frozen soils, Global Planet Change, 29, 275-292, 10.1016/S0921-8181(01)00095-9, 2001.

Kienzler, P. M., and Naef, F.: Subsurface storm flow formation at different hillslopes and implications for the 'old water paradox', Hydrological Processes, 22, 104-116, 10.1002/hyp.6687, 2008.

Kirchner, J. W.: A double paradox in catchment hydrology and geochemistry, Hydrological Processes, 17, 871-874, 10.1002/hyp.5108, 2003.

Landais, A., Barkan, E., and Luz, B.: Record of delta O-18 and O-17-excess in ice from Vostok Antarctica during the last 150,000 years, Geophys Res Lett, 35, 10.1029/2007gl032096, 2008.

Landais, A., Barkan, E., Yakir, D., and Luz, B.: The triple isotopic composition of oxygen in leaf water, Geochim Cosmochim Ac, 70, 4105-4115, 10.1016/j.gca.2006.06.1545, 2006.

1010   Landwehr, J. M. and Coplen, T. B.: Line-conditioned excess: a new method for characterizing stable hydrogen and oxygen isotope ratios in hydrologic systems, International Conference on Isotopes in Environmental Studies, Aquatic Forum, Monte-Carlo, Monaco, 25–29 October 2004, IAEA, Vienna, 132–135, 2006.

Lane, S. N., Borgeaud, L., and Vittoz, P.: Emergent geomorphic-vegetation interactions on a subalpine alluvial fan, Earth Surface Processes and Landforms, 41, 72-86, 10.1002/esp.3833, 2016.

1015   Leuenberger, M. C. and Ranjan, S.: Disentangle Kinetic From Equilibrium Fractionation Using Primary (delta O-17, delta O-18, delta D) and Secondary (Delta O-17, d(ex)) Stable Isotope Parameters on Samples From the Swiss Precipitation Network, Front Earth Sc-Switz, 9, 10.3389/feart.2021.598061, 2021.

Linsbauer, A., Huss, M., Hodel, E., Bauder, A., Fischer, M., Weidmann, Y., Bärtschi, H., and Schmassmann, E.: The new Swiss Glacier Inventory SGI2016: From a topographical to a glaciological dataset, Frontiers in Earth Science, in review, 1020   10.5194/egusphere-egu21-5873, 2021.

Livneh, B. and Badger, A. M.: Drought less predictable under declining future snowpack, Nat. Clim. Chang., 10, 452-+, 10.1038/s41558-020-0754-8, 2020.

Lucianetti, G., Penna, D., Mastrorillo, L., and Mazza, R.: The Role of Snowmelt on the Spatio-Temporal Variability of Spring Recharge in a Dolomitic Mountain Group, Italian Alps, Water, 12, 26, 10.3390/w12082256, 2020.

1025   Mächler, E., Salyani, A., Walser, J. C., Larsen, A., Schaefli, B., Altermatt, F., and Ceperley, N.: Environmental DNA simultaneously informs hydrological and biodiversity characterization of an Alpine catchment, Hydrol. Earth Syst. Sci., 1-30, 10.5194/hess-25-735-2021, 2021.

Majoube, M.: Fractionnement en oxygène 18 et en deutérium entre l'eau et sa vapeur, J. Chim. Phys., 68, 1423-1436, 1971.

McDonnell, J. J. (1990), A rationale for old water discharge through macropores in a steep, humid catchment, Water 1030   Resour. Res., 26, 2821–2832.

McDonnell, J. J., McGuire, K., Aggarwal, P., Beven, K. J., Biondi, D., Destouni, G., Dunn, S., James, A., Kirchner, J., Kraft, P., Lyon, S., Maloszewski, P., Newman, B., Pfister, L., Rinaldo, A., Rodhe, A., Sayama, T., Seibert, J., Solomon, K., Soulsby, C., Stewart, M., Tetzlaff, D., Tobin, C., Troch, P., Weiler, M., Western, A., Wörman, A., and Wrede, S.: How old is streamwater? Open questions in catchment transit time conceptualization, modelling and analysis, 1035   Hydrological Processes, 24, 1745-1754, 10.1002/hyp.7796, 2010.

Meijer, H. A. J. and Li, W. J.: The use of electrolysis for accurate delta O-17 and delta O-18 isotope measurements in water, Isot Environ Healt S, 34, 349-369, 10.1080/10256019808234072, 1998.

MeteoSwiss: Documentation of MeteoSwiss Grid-Data Products: Daily Precipitation (final analysis): RhiresD, 2019.

Michelon, A.: Hydrologic processes analysis in a high Alpine catchment: the case of the Vallon de Nant, PhD thesis, 1040   University of Lausanne, Lausanne, https://serval.unil.ch/resource/serval:BIB_0C61AF744730.P002/REF.pdf, 2022.

Michelon, A, Ceperley, N, Beria, H., Larsen, J., Schaefli, B., Venneman, T., 2862 water samples from Vallon de Nant analyzed for stable water isotopes (dD, d17O, d18O) and electric conductivity. Zenodo, 10.5281/zenodo.5940044, 2022

Michelon, A., Schaefli, B., Ceperley, N., and Beria, H.: Weather dataset from Vallon de Nant, Switzerland (from 16 August 2016 to 14 October 2018), Zenodo, 10.5281/zenodo.5518942, 2021a.

1045   Michelon, A., Benoit, L., Beria, H., Ceperley, N., and Schaefli, B.: Benefits from high-density rain gauge observations for hydrological response analysis in a small alpine catchment, Hydrol. Earth Syst. Sci., 25, 2301-2325, 10.5194/hess-25-2301-2021, 2021b.

Miralha, L., Wissler, A. D., Segura, C., and Bladon, K. D.: Characterizing stream temperature hysteresis in forested headwater streams, Hydrological Processes, 37, e14795, 10.1002/hyp.14795, 2023.

1050   Mosquera, G. M., Segura, C., Vaché, K. B., Windhorst, D., Breuer, L., and Crespo, P.: Insights into the water mean transit time in a high-elevation tropicalecosystem, Hydrology and Earth System Sciences, 20, 2987-3004, 10.5194/hess-20-2987-2016, 2016.

1055 Muelchi, R., Rossler, O., Schwanbeck, J., Weingartner, R., and Martius, O.: River runoff in Switzerland in a changing climate - runoff regime changes and their time of emergence, Hydrology and Earth System Sciences, 25, 3071-3086, 10.5194/hess-25-3071-2021, 2021.

Musselman, K. N., Addor, N., Vano, J. A., and Molotch, N. P.: Winter melt trends portend widespread declines in snow water resources, Nat. Clim. Chang., 11, 17, 10.1038/s41558-021-01014-9, 2021.

Nyamgerel, Y., Han, Y., Kim, M., Koh, D., and Lee, J.: Review on Applications of O-17 in Hydrological Cycle, Molecules, 26, 10.3390/molecules26154468, 2021.

1060 Ochsner, T. E., Horton, R., and Ren, T. H.: A new perspective on soil thermal properties, Soil Science Society of America Journal, 65, 1641-1647, 10.2136/sssaj2001.1641, 2001.

Ohlanders, N., Rodriguez, M., and McPhee, J.: Stable water isotope variation in a Central Andean watershed dominated by glacier and snowmelt, Hydrol. Earth Syst. Sci., 17, 1035-1050, 10.5194/hess-17-1035-2013, 2013.

Penna, D., Engel, M., Bertoldi, G., and Comiti, F.: Towards a tracer-based conceptualization of meltwater dynamics and
1065 streamflow response in a glacierized catchment, Hydrology and Earth System Sciences, 21, 23-41, 10.5194/hess-21-23-2017, 2017.

Penna, D., van Meerveld, H. J., Zuecco, G., Fontana, G. D., and Borga, M.: Hydrological response of an Alpine catchment to rainfall and snowmelt events, J. Hydrol., 537, 382-397, 10.1016/j.jhydrol.2016.03.040, 2016.

Penna, D., Engel, M., Mao, L., Dell'Agnese, A., Bertoldi, G., and Comiti, F.: Tracer-based analysis of spatial and temporal
1070 variations of water sources in a glacierized catchment, Hydrol. Earth Syst. Sci., 18, 5271-5288, 10.5194/hess-18-5271-2014, 2014.

Penna, D., Stenni, B., Šanda, M., Wrede, S., Bogaard, T. A., Michelini, M., Fischer, B. M. C., Gobbi, A., Mantese, N., Zuecco, G., Borga, M., Bonazza, M., Sobotková, M., Čejková, B., and Wassenaar, L. I.: Technical Note: Evaluation of between-sample memory effects in the analysis of f $\delta2H$ and $\delta18O$ of of water samples measured by laser spectroscopes,
1075 Hydrology and Earth System Sciences, 16, 3925-3933, 10.5194/hess-16-3925-2012, 2012.

Risi, C., Landais, A., Bony, S., Jouzel, J., Masson-Delmotte, V., and Vimeux, F.: Understanding the O-17 excess glacial-interglacial variations in Vostok precipitation, J Geophys Res-Atmos, 115, 10.1029/2008jd011535, 2010.

Rowley, M. C., Grand, S., and Verrecchia, E. P.: Calcium-mediated stabilisation of soil organic carbon, Biogeochemistry, 137, 27-49, 10.1007/s10533-017-0410-1, 2018.

1080 Rucker, A., Zappa, M., Boss, S., and von Freyberg, J.: An optimized snowmelt lysimeter system for monitoring melt rates and collecting samples for stable water isotope analysis, J. Hydrol. Hydromech., 67, 20-31, 10.2478/johh-2018-0007, 2019.

Rücker, A., Boss, S., Kirchner, J. W., and von Freyberg, J.: Monitoring snowpack outflow volumes and their isotopic composition to better understand streamflow generation during rain-on-snow events, Hydrology and Earth System
1085 Sciences, 23, 2983-3005, 10.5194/hess-23-2983-2019, 2019.

Santos, A. C., Portela, M. M., Rinaldo, A., and Schaefli, B.: Analytical flow duration curves for summer streamflow in Switzerland, Hydrology and Earth System Sciences, 22, 2377-2389, 10.5194/hess-22-2377-2018, 2018.

Schaefli, B.: Average daily air temperature, precipitation and relative sunshine duration for Vallon de Nant catchment, extracted from gridded MeteoSwiss data (1961-2020), Zenodo, 10.5281/zenodo.5420415, 2021.

1090 Schaefli, B., Rinaldo, A., and Botter, G.: Analytic probability distributions for snow-dominated streamflow, Water Resources Research, 49, 1-13, 10.1002/2012WR020234, 2013.

Schaefli, B., Nicotina, L., Imfeld, C., Da Ronco, P., Bertuzzo, E., and Rinaldo, A.: SEHR-ECHO v1.0: a Spatially Explicit Hydrologic Response model for ecohydrologic applications, Geosci Model Dev, 7, 2733-2746, 10.5194/gmd-7-2733-2014, 2014.

1095   Schauer, A. J., Schoenemann, S. W., and Steig, E. J.: Routine high-precision analysis of triple water-isotope ratios using cavity ring-down spectroscopy, Rapid Commun Mass Sp, 30, 2059-2069, 10.1002/rcm.7682, 2016.

Schotterer, U., Stichler, W., and Ginot, P.: The Influence of Post-Depositional Effects on Ice Core Studies: Examples From the Alps, Andes, and Altai, Springer Netherlands, 10.1007/1-4020-2146-1_3, 2004.

Schurch, M., Kozel, R., Schotterer, U., and Tripet, J. P.: Observation of isotopes in the water cycle - the Swiss National
1100   Network (NISOT), Environ Geol, 45, 1-11, 10.1007/s00254-003-0843-9, 2003.

Sodemann, H. and Zubler, E.: Seasonal and inter-annual variability of the moisture sources for Alpine precipitation during 1995-2002, Int. J. Climatol., 10.1002/joc.1932, 2009.

Sprenger, M., Leistert, H., Gimbel, K., and Weiler, M.: Illuminating hydrological processes at the soil-vegetation-atmosphere interface with water stable isotopes, Reviews of Geophysics, 54, 2015RG000515, 10.1002/2015RG000515,
1105   2016.

Staudinger, M., Stoelzle, M., Seeger, S., Seibert, J., Weiler, M., and Stahl, K.: Catchment water storage variation with elevation, 31, 2000-2015, 10.1002/hyp.11158, 2017.

Surma, J., Assonov, S., and Staubwasser, M.: Triple Oxygen Isotope Systematics in the Hydrologic Cycle,, Reviews in Mineralogy and Geochemistry, 401–428, 10.2138/rmg.2021.86.12, 2021.

1110   swissAlti3D: The digital elevation model of Switzerland, 2012.

The MathWorks, I.: Curve Fitting Toolbox, https://www.mathworks.com/products/curvefitting.html, 2017.

Thornton, J. M.: Fully-integrated hydrological modelling in steep, snow-dominated, geologically complex Alpine terrain, PhD Thesis, University of Neuchâtel, Switzerland, https://libra.unine.ch/Publications/James_Thornton/49031, 2020.

Thornton, J. M., Brauchli, T., Mariethoz, G., and Brunner, P.: Efficient multi-objective calibration and uncertainty analysis
1115   of distributed snow simulations in rugged alpine terrain, J. Hydrol., 126241, 10.1016/j.jhydrol.2021.126241, 2021a.

Thornton, J. M., Therrien, R., Mariéthoz, G., Linde, N., and Brunner, P.: Simulating fully-integrated hydrological dynamics in complex Alpine headwaters, EarthArXiv, pre-print, 10.31223/X5RG7Q, 2021b.

Tian, C., Wang, L., Kaseke, K. F., and Bird, B. W.: Stable isotope compositions (δ2H, δ18O and δ17O) of rainfall and snowfall in the central United States, Scientific Reports, 8, 10.1038/s41598-018-25102-7, 2018.

1120   Trask, J. C., Devine, S. M., and Fogg, G. E.: Soil temperature survey in a mountain basin, Geoderma, 367, 114202, 10.1016/j.geoderma.2020.114202, 2020.

Vallet-Coulomb, C., Couapel, M., and Sonzogni, C.: Improving memory effect correction to achieve high-precision analysis of δ17O, δ18O, δ2H, 17O-excess and d-excess in water using cavity ring-down laser spectroscopy, Rapid Commun Mass Sp, 35, e9108, 10/gqd2zg, 2021.

1125   Vittoz, P.: Permanent.Plot.ch – a database for Swiss permanent vegetation plots, Biodiversity & Ecology, 4, 337-337, 10.7809/b-e.00128, 2012.

Vittoz, P.: Soil temperature series in Vallon de Nant catchment, Switzerland, Zenodo, 10.5281/zenodo.4715669, 2021.

von Freyberg, J., Knapp, J. L. A., Rücker, A., Studer, B., and Kirchner, J. W.: Technical note: Evaluation of a low-cost evaporation protection method for portable water samplers, Hydrology and Earth System Sciences, 24, 5821-5834,
1130   10.5194/hess-24-5821-2020, 2020.

Webb, R. W., Wigmore, O., Jennings, K., Fend, M., and Molotch, N. P.: Hydrologic connectivity at the hillslope scale through intra-snowpack flow paths during snowmelt, Hydrological Processes, 34, 1616-1629, 10.1002/hyp.13686, 2020.

Wei, Z. W., Lee, X., Aemisegger, F., Benetti, M., Berkelhammer, M., Casado, M., Caylor, K., Christner, E., Dyroff, C., Garcia, O., Gonzalez, Y., Griffis, T., Kurita, N., Liang, J., Liang, M. C., Lin, G. H., Noone, D., Gribanov, K.,
1135   Munksgaard, N. C., Schneider, M., Ritter, F., Steen-Larsen, H. C., Vallet-Coulomb, C., Wen, X. F., Wright, J. S., Xiao,

W., and Yoshimura, K.: A global database of water vapor isotopes measured with high temporal resolution infrared laser spectroscopy, Sci Data, 6, 10.1038/sdata.2018.302, 2019.

Zuecco, G., Carturan, L., De Blasi, F., Seppi, R., Zanoner, T., Penna, D., Borga, M., Carton, A., and Dalla Fontana, G.: Understanding hydrological processes in glacierized catchments: Evidence and implications of highly variable isotopic and electrical conductivity data, Hydrological Processes, 33, 816-832, 10.1002/hyp.13366, 2019.

1140